Protein kinase D1/2 is involved in the maturation of multivesicular bodies and secretion of exosomes in T and B lymphocytes

Carla Mazzeo[¶], Víctor Calvo[¶], Roberto Alonso[¶], Isabel Mérida[+] and Manuel Izquierdo[¶*]

[¶]Departamento de Bioquímica. Instituto de Investigaciones Biomédicas Alberto Sols CSIC-UAM Madrid and [+]Department of Immunology & Oncology, Centro Nacional de Biotecnología CSIC, Madrid, Spain

Running title: PKD1/2 regulates exosome secretion

[*]**Correspondence:** Manuel Izquierdo

Instituto de Investigaciones Biomédicas Alberto Sols, Lab C-20

CSIC-Universidad Autónoma de Madrid

Arturo Duperier 4

28029 Madrid, Spain

e-mail: mizquierdo@iib.uam.es

Tel: +34 91 4973117

Fax: +34 91 5854401

Abstract

Multivesicular bodies (MVB) are endocytic compartments that enclose intraluminal vesicles (ILV) formed by inward budding from the limiting membrane of endosomes. In T lymphocytes, these ILV contain Fas ligand (FasL) and are secreted as "lethal exosomes" following activation-induced fusion of the MVB with the plasma membrane. Diacylglycerol (DAG) and diacylglycerol kinase α (DGKα) regulate MVB maturation and polarized traffic as well as subsequent secretion of pro-apoptotic exosomes, but the molecular basis underlying these phenomena remains unclear. Here we identify protein kinase D (PKD) family members as DAG effectors involved in MVB genesis and secretion. We show that the inducible secretion of exosomes is enhanced when a constitutively active PKD1 mutant is expressed in T lymphocytes, whereas exosome secretion is impaired in PKD2-deficient mouse T lymphoblasts and in PKD1/3-null B cells. Analysis of PKD2-deficient T lymphoblasts showed the presence of large, immature MVB-like vesicles and demonstrated defects in cytotoxic activity and in activation-induced cell death. Using pharmacological and genetic tools, we show that DGKα regulates PKD1/2 subcellular localization and activation. Our studies demonstrate that PKD1/2 is a key regulator of MVB maturation and exosome secretion, and constitutes a mediator of the DGKα effect on MVB secretory traffic.

WORDS: INTRO+RES+DIS = (3875)

Key words: Diacylglycerol kinase, cytotoxic activity, activation-induced cell death, polarization, immune synapse, membrane traffic

Abbreviations: AICD, activation-induced cell death; APC; antigen-presenting cell; CMAC, cell tracker blue; CTL; cytotoxic T lymphocyte; DAG, diacylglycerol; DGKα, diacylglycerol kinase α; ESCRT, endosomal complex required for traffic; FasL, Fas ligand; ILV, intraluminal vesicles; HM1R, muscarinic receptor; IS; immune synapse; MVB, multivesicular bodies; PA, phosphatidic acid; PBL, peripheral blood lymphocytes; PKC, protein kinase C; PKD, protein kinase D; PLC, phospholipase C; PMA, phorbol myristate acetate; SEE, Staphylococcus enterotoxin E; SEB, Staphylococcus enterotoxin B; TGN, *trans*-Golgi network

Introduction

Exosomes are nanovesicles (40-100 nm) that form as intraluminal vesicles (ILV) inside multivesicular bodies (MVB) and are then secreted by numerous cell types.[1] ILV are generated by inward budding of late endosome limiting membrane in a precisely regulated maturation process.[2, 3] Two main pathways are involved in MVB maturation.[4, 5] The most likely candidates for the molecular machinery that drives MVB maturation are the ESCRT (endosomal complex required for traffic) proteins;[6] there is nonetheless increasing evidence that lipids such as lyso-bisphosphatidic acid (LBPA),[7] ceramides[8] and diacylglyerol (DAG)[9] have a key role in this membrane invagination process.

Exosomes participate in many biological processes related to TCR (T cell receptor)-triggered immune responses, including T lymphocyte-mediated cytotoxicity and activation-induced cell death (AICD), antigen presentation, and intercellular miRNA exchange.[10, 11, 12, 13, 14, 15] The discovery of exosome involvement in these responses increased interest in the regulation of exosome biogenesis and secretory traffic, with special attention to the contribution of lipids such as ceramide and DAG, as well as DAG-binding proteins.[14, 16, 17, 18, 19, 20, 21] These studies suggest that positive and negative DAG regulators might control secretory traffic. By transforming DAG into phosphatidic acid (PA), diacylglycerol kinase α (DGKα) is essential for the negative control of DAG function in T lymphocytes.[22] DGKα translocates transiently to the T cell membrane after muscarinic receptor (HM1R) triggering or to the immune synapse (IS) after TCR stimulation; at these subcellular locations, DGKα acts as a negative modulator of phospholipase C (PLC)-generated DAG.[23, 24] Transient DGKα relocalization from cytosol to the plasma membrane to gain access to its substrate appears to be the limiting event that controls DAG-regulated functions.[23]

The secretory vesicle pathway involves several DAG-controlled checkpoints at which DGKα might act; these include vesicle formation and fission at the *trans*-Golgi network

(TGN), MVB generation and maturation as well as their transport, docking, and fusion to the plasma membrane.[9, 16, 17, 18, 19, 20] The molecular components and control elements that regulate some of these trafficking processes include protein kinase D (PKD) family members.[21] PKD1 activity, for instance, regulates fission of transport vesicles from TGN via direct interaction with the pre-existing DAG pool at this site.[19] The cytosolic serine/threonine kinases PKD1, PKD2 and PKD3 (ref. 21) are expressed in a wide range of cells, with PKD2 the most abundant isotype in T lymphocytes.[25, 26] PKD have two DAG-binding domains (C1a, C1b) at the N terminus,[21] which mediate PKD recruitment to cell membranes. PKC phosphorylation at the PKD activation loop further promotes PKD autophosphorylation and activation.[27]

Based on our previous studies showing DGKα regulation of DAG in MVB formation and exosome secretion,[9, 14, 28] and the identification of PKD1/2 association to MVB,[14] we hypothesized that DGKα control of DAG mediates these events, at least in part, through PKD. Here we explored whether, in addition to its well-characterized role in vesicle fission from TGN,[19] PKD regulates other steps in the DAG-controlled secretory traffic pathway. Using PKD-deficient cell models, we analyzed the role of PKD1/2 in MVB formation and function, and demonstrate their implication in exosome secretory traffic.

Results

Pharmacological PKC inhibition limits exosome secretion in T lymphocytes

DGKα limits exosome secretion in T lymphocytes in a non-polarized model (anti-TCR or carbachol (CCh) activation of human T lymphoblasts or Jurkat J-HM1-2.2 cells)[14, 28] and in a polarized secretion model (induction by SEE superantigen-loaded Raji cells).[9] This negative effect correlates with exosome secretion induced by addition of the cell-permeable DAG analogue dioctanoyl glycerol (DOG).[14]

To assess the role of PKD in exosome secretion, we first inhibited its upstream activator PKC using RO318220, a broad range PKC inhibitor that prevents TCR- and phorbol myristate acetate (PMA)-induced PKD phosphorylation by PKC[29]. To test RO318220 efficiency, we analyzed PMA-induced, PKC-dependent phosphorylation of endogenous PKD1/2 and of PKD1 fused to GFP (green fluorescent protein; GFP-PKD1) at the activation loop (pS744/S748)[30] (Supplementary Figure S1A); the effect was similar in cells that express a PKD1 kinase-deficient mutant (D733A; GFP-PKD1KD).[19, 31] In addition, we analyzed inhibition by measuring autophosphorylation (pS916)[27, 29] induced by CCh (Supplementary Figure S1B) or by anti-TCR (not shown). We pretreated J-HM1-2.2 cells with RO318220, followed by anti-TCR antibody or CCh stimulation to induce exosome secretion.[14] Exosomes isolated from culture supernatants[14, 32, 33, 34] were quantitated by WB using anti-CD63 or by NANOSIGHT, with similar results (Supplementary Figure S2). In supernatants of cells pre-treated with RO318220 and stimulated with anti-TCR or CCh, we found a notable decrease in exosomal CD63 and FasL (Figures 1A, B). These results suggest that reducing PKC-dependent, PKD activation by RO318220 treatment results in less CD63 and FasL secretion into exosomes with a comparable decrease in the number of exosomes secreted (particles/ml culture supernatant; Figure 1C).

PKD1/2 regulate exosome secretion in T lymphocytes

Although PKC inhibition can have many effects in addition to PKD inhibition, our observations are compatible with PKC and/or PKD involvement in exosome biogenesis/secretion. For its activation, PKD requires both direct DAG recognition as well as DAG-triggered PKC-dependent phosphorylation. To analyze PKD function in more detail, we used an exosome reporter secretion assay[9, 14] based on transient expression of the exosome reporter DsRed2-CD63 and several GFP-PKD1 constructs, including GFP-PKD1, GFP-PKD1KD and a GFP-PKD1 version with phospho-mimetic glutamic residues that replace the PKC phosphorylation sites at S744/748 (GFP-PKD1CA). We analyzed exosome secretion by WB with anti-CD63 (Figure 2A, top). We normalized the results to the transfection efficiency of the exosome reporter and the number of viable exosome-secreting cells by WB analysis of total cell lysates using anti-CD63 and anti-β-actin (Figure 2A, bottom).

CCh stimulation induced exosome secretion; this effect was increased by pretreatment with the DGKα inhibitor R59949 (ref. 9, 14). GFP-PKD1WT expression did not markedly alter CCh-induced exosome secretion, whereas the GFP-PKD1KD mutant, which acts as a PKD1 dominant-inhibitory mutant,[19] impaired exosome secretion even in the presence of the inhibitor (Figure 2B). These experiments support an endogenous PKD contribution to exosome secretion. The lack of effect due to GFP-PDK1WT expression also suggests that DAG generation, directly or through PKC-dependent phosphorylation, is a limiting factor in PKD activation. For its activation, the GFP-PKD1CA mutant bypasses the PKC phosphorylation requirement, but not that for PLC-generated DAG.[19, 31] GFP-PKD1CA-expressing cells showed enhanced exosome secretion in response to CCh stimulation compared to GFP-PKD1WT-expressing cells (Figure 2B). This finding shows the importance of PKD phosphorylation by PKC for exosome secretion. Treatment with the DGKα inhibitor further increased exosome secretion by GFP-PKD1CA-expressing cells,

which suggests that DGKα consumption of DAG controls PKD activation, not only through PKC phosphorylation, but also through direct DAG binding.

We compared exosome secretion by the J-HM1-2.2 cell line with that of primary cells, using WB of endogenous and chimeric CD63 and by NANOSIGHT measurements of human T lymphocyte types using various stimuli (CCh and anti-TCR for J-HM1-2.2 cells; anti-TCR for T lymphoblasts and peripheral blood lymphocytes, PBL) (Figure 2C). T lymphoblasts and J-HM1-2.2 cells secreted comparable exosome numbers after TCR triggering, whereas exosome secretion by PBL was not enhanced following stimulation. Inhibition of DGKα enhanced exosome secretion in stimulated J-HM1-2.2 cells and T lymphoblasts (Figure 2C).

To evaluate the PKD1 effect on polarized exosome secretion in an IS model, we challenged GFP-CD63-expressing Jurkat cells with SEE-presenting Raji B cells[35], which allowed analysis of GFP-CD63$^+$ MVB traffic and exosome secretion[9]. Following conjugate formation, intracellular GFP-CD63$^+$ MVB accumulated in Jurkat cells at the synapse contact area (Supplementary Video 1; interacting cells, top right), but not in unconjugated Jurkat cells (GFP-CD63-expressing cells; bottom left). MVB movement and concentration in the synapse area was recorded at 2 h post-conjugate formation (Supplementary Video 2) and vesicle trajectories plotted (Figure 3A). Although the vesicles showed apparent random movement in conjugated cells, they tended to tether near the synapse contact area (Figure 3A). To examine exosome secretion, we challenged Jurkat cells co-expressing GFP-CD63 and GFP-PKD1CA with Raji cells, untreated or SEE-pulsed (Supplementary Video 1). After synapse formation, we analyzed GFP-CD63$^+$ exosomes, and expressed the results as normalized *x*-fold induction (Figure 3B). Expression of the GFP-PKD1CA mutant enhanced exosome secretion compared with an irrelevant control (GFP). PKD thus appears

to be involved in activation-induced exosome secretion in T lymphocytes in polarized and non-polarized secretion models.

PKD1 regulates exosome secretion in a B cell model

B cell receptor stimulation with anti-IgM (M4 antibody) activates PKD1 and PKD3 (ref. 36) and induces secretion of $CD63^+$ exosomes, which participate in antigen presentation.[37, 38, 39, 40] To extend results from T lymphocytes to B cells, we studied exosome secretion in DT40 chicken B lymphocytes that lacked their two PKD isotypes, PKD1 and PKD3.[36] Wild type and $PKD1^{-/-}3^{-/-}$ DT40 cells were transfected with GFP-CD63 and exosome secretion was assessed after stimulation with PMA plus ionomycin or with anti-IgM. PMA plus ionomycin induced exosome secretion in WT, but not in $PKD1^{-/-}3^{-/-}$ DT40 cells (Figure 4A). $PKD1^{-/-}3^{-/-}$ cells bore a doxycycline-inducible Flag-tagged PKD3 transgene that, in the presence of tetracycline, induced Flag-PKD3 expression at levels comparable to those of endogenous PKD3 in WT DT40 cells[36, 41] (Supplementary Figure S3). To determine the functional redundance of PKD1 and PKD3 in exosome secretion control, we induced Flag-PKD3 expression and stimulated WT, $PKD1^{-/-}3^{-/-}$, and $PKD1^{-/-}$ DT40 cells with anti-IgM. In Flag-PKD3-expressing ($PKD1^{-/-}$) DT40 cells, exosome secretion was not restored to the levels of WT DT40 controls (Figure 4B, C). Western blot results were comparable when we analyzed endogenous CD63 in exosomes secreted by WT and $PKD1^{-/-}$ DT40 cells (Figure 4D, E). When GFP-PKD1 was expressed in $PKD1^{-/-}3^{-/-}$ cells to yield $PKD3^{-/-}$ DT40 cells, inducible exosome secretion was rescued to the values observed for WT DT40 cells (Figure 4F). PKD1 thus appears to be the essential isoform for inducible exosome secretion in chicken B lymphocytes.

PKD2 regulates exosome secretion in primary T lymphocytes

PKD2 is the main PKD isotype in human and mouse T lymphocytes.[25, 26] We therefore analyzed T lymphoblasts from mice that lacked PKD2 (ref. 26) to determine its contribution

to MVB traffic and exosome secretion. T lymphoblasts from WT and PKD2$^{-/-}$ mice were retrovirally transduced to express GFP-CD63, and then stimulated for 18 h with plate-bound anti-TCR to induce secretory traffic of MVB. Live-cell imaging of transduced WT T lymphoblasts showed numerous GFP-CD63^{+} vesicles with apparently random movement within the cell, as well as weak cell surface fluorescence that might reflect constitutive CD63 traffic[42] (Supplementary Video 3). Following TCR stimulation, we consistently observed increased fluorescence at the plasma membrane, a finding compatible with GFP-CD63^{+} MVB degranulation[43, 44] (Supplementary Video 4). After stimulation, some of these vesicles approached and apparently docked to the plasma membrane. Fluorescence at the docking point increased transiently and was later lost (Supplementary Video 5, trajectories 1 and 2; Supplementary Figure S4), suggesting TCR-induced MVB fusion to the plasma membrane.

The increase in cell surface GFP-CD63 after TCR stimulation was probably due to GFP-CD63 transfer from the MVB limiting membrane to the T cell plasma membrane (Supplementary Video 5, Figure 5A). The ratio of plasma membrane to total GFP-CD63 fluorescence intensity after TCR stimulation increased similarly in PKD2$^{-/-}$ and WT T lymphoblasts (Figure 5A). Lack of PKD2 therefore did not alter TCR-induced MVB docking and fusion. After TCR stimulation, the mean velocity of CD63^{+} MVB was also similar in PKD2$^{-/-}$ and WT T lymphoblasts (not shown). Several crucial steps in MVB trafficking (transport, docking, and fusion) thus appeared to be unaffected by PKD2 deficiency. In contrast, WB analysis showed lack of inducible exosome secretion in PKD2$^{-/-}$ T lymphoblasts (Figure 5B). PKD2 reconstitution of PKD2$^{-/-}$ T lymphoblasts enhanced TCR-triggered exosome secretion compared to PKD2$^{-/-}$ or WT T lymphoblasts (Figure 5C).

PKD involvement in MVB morphogenesis

DGKα enzyme activity negatively regulates MVB maturation, as does expression of VPS4EQ, an ATPase-defective mutant of vacuolar protein sorting 4 that cooperates with the ESCRT complex.[9] Immature MVB consist of enlarged, ring-shaped $CD63^+$ endocytic vesicles with no ILV.[46] The molecular basis of the DGKα effect on MVB maturation is unclear, as DGKα is not known to regulate any ESCRT protein. PKD1/2 regulate exosome secretion by T and B lymphocytes (Figures 4, 5), but do not affect MVB velocity or docking/fusion to the plasma membrane (not shown and Figure 5). $PKD2^{-/-}$ T lymphoblasts showed enlarged $CD63^+$ vesicles with an anomalous, ring-shaped structure (Figure 5A, bottom; Supplementary Video 6), which suggests that PKD2 participates in MVB maturation. Quantitative analysis showed clear differences in vesicle area in TCR-stimulated WT vs. $PKD2^{-/-}$ T lymphoblasts (not shown).

PI3K/Vps34 (phosphatidyl-inositol-3-phosphate kinase/vacuolar protein sorting 34) is a regulator of the ESCRT complex that participates in MVB maturation.[45, 46] PI3K inhibition thus limits MVB maturation.[45, 47, 48, 49] WT and $PKD1^{-/-}3^{-/-}$ GFP-$CD63^+$ DT40 cells were incubated alone or with the PI3K inhibitor LY294002. Inhibitor-treated WT DT40 cells formed a cluster of enlarged, ring-shaped $CD63^+$ vesicles morphologically similar to those found constitutively in $PKD1^{-/-}3^{-/-}$ DT40 cells (Figure 6A). $CD63^+$ vesicles were comparable in size and shape in untreated and PI3K inhibitor-treated $PKD1^{-/-}3^{-/-}$ DT40 cells (Figure 6A), and were similar to those in $PKD2^{-/-}$ T lymphoblasts (Figures 5A, 6B, Supplementary Video 6). These data demonstrate that PKD regulates exosome secretion, at least in part through control of MVB morphogenesis.

DGKα regulates PKD1/2 activation

PKD positively controls MVB maturation and exosome secretion, whereas DGKα enzyme activity negatively regulates these processes,[9] and the DGKα inhibitor did not rescue GFP-PKD1KD mutant inhibition of exosome secretion (Figure 2B). DGKα might

thus control PKD1 activation in a pathway that governs MVB maturation/exosome secretion. We analyzed this possibility using J-HM1-2.2 cells alone or treated with the DGKα inhibitor R59949, and activated with CCh, anti-TCR, or anti-TCR plus anti-CD28. WB analysis of R59949-treated cells showed an increase in active PKD1/2, as measured by phosphorylation on its activation loop (S744/S748). This increase was most evident from 30 min to 3 h post-stimulation (Figure 7A). R59949 treatment did not enhance PMA-induced PKD1/2 phosphorylation (not shown), indicating that the effect was specific for the TCR and HM1R, which activate PKD1/2 via PLC-generated DAG.

To test whether DGKα overexpression affects PKD1/2 activation, we transfected J-HM1-2.2 cells with DsRed2-PKD1 alone or cotransfected with GFP-DGKα, and stimulated them with CCh or PMA plus ionomycin (which induces DAG-independent PKD1/2 activation). WB analysis with anti-(pS744/748)PKD1/2 showed less DsRed2-PKD1 and endogenous PKD1/2 phosphorylation in CCh-treated, GFP-DGKα and DsRed2-PKD1 co-expressing cells than in cells that expressed DsRed2-PKD1 alone. This phosphorylation difference was not observed in PMA plus ionomycin-stimulated cells (Figure 7B).

We tested the effect of attenuating endogenous DGKα expression on PKD activation in the IS model. In confocal microscopy experiments, we validated the (pS916)PKD1/2 antibody by stimulating Jurkat cells with PMA or SEE-pulsed Raji cells to induce synapse formation (Fig. 8A); stimulation led to an increase in (pS916)PKD1/2 signal, which co-localized with CD63 (PMA) or synaptic membrane area (SEE-pulsed Raji cells). We reduced DGKα expression by transfecting Jurkat cells with a bicistronic siRNA interference vector bearing GFP-coding sequence and DGKα–specific siRNA.[9] This approach allowed single-cell comparison of PKD1/2 activation in DGKα-silenced GFP^+ cells with control GFP^- cells during synapse formation (Figure 8B, top). Using image quantification of synapses, we compared the frequency distributions of PKD1/2 activation in synapses formed

by DGKα-silenced cells and unsilenced Jurkat cells (Figure 8B, bottom). DGKα attenuation enhanced PKD activation, as indicated by an increase in mean fluorescence intensity of (pS916)PKD1/2 at the synaptic membrane. Since PKD1 recruitment to the synapse depends on transient DAG production at this site, we measured DsRed2-PKD1 residence half-time at the synapse in DGKα-silenced cells by time-lapse video analysis (Supplementary Video 7). DGKα attenuation significantly enhanced mean DsRed2-PKD1 residence half-time at the synaptic membrane from 15-20 to 40 min (Supplementary Figure S5). DAG consumption by DGKα could thus negatively control PKD1/2 recruitment to and activation at the IS.

PKD2 controls CTL activity and AICD in T lymphoblasts

Since PKD appears to be necessary for MVB secretory traffic and exosome secretion, we examined the effect of PKD2 deficiency on cytotoxic T lymphocyte activity (CTL) and AICD of T lymphoblasts. CTL cytotoxic granules have a MVB structure and contain perforin, granzymes and FasL;[44] internal vesicles from these MVB are released to the synaptic cleft as exosomes.[10] MVB degranulation and FasL secretion on exosomes mediates AICD of $CD4^+$ T lymphocytes and Jurkat cells.[33, 14] To test the PKD2 effect on control of CTL activity and AICD, we used a murine IS model in which TCR-stimulated T lymphoblasts were challenged with SEB-pulsed, CMAC-labeled EL-4 cells. SEB binds to Vβ3,7,8,17-TCR-bearing T cells, which in mice make up a large proportion (~30%) of T lymphocytes,[50] and induces T cell activation and AICD.[51] EL-4 syngeneic cells and their variants are used as target cells in murine CTL assays,[52, 53] but also induce reactivation and AICD of effector T lymphocytes. After several transient synaptic contacts, $CMAC^+$ EL-4 cells and T lymphoblasts both underwent apoptosis (plasma membrane blebbing; Supplementary Video 8). In mixed cultures at various effector:target/stimulator ratios, we used flow cytometry to quantitate the percentage of apoptosis (annexin V^+ cells) in EL-4 cells (CTL activity marker) or T lymphoblasts (AICD marker) (Figure 9). CTL activity in

response to SEB-pulsed EL-4 cells was lower in PKD2$^{-/-}$ than in WT T lymphoblasts, with a concomitant decrease in AICD in PKD2$^{-/-}$ versus WT T lymphoblasts (Figure 9, top). Since only 30% of mouse T lymphoblasts express the SEB-responsive Vβ TCR, we restimulated T lymphoblasts with polyclonal anti-TCR to induce more extensive cell death; AICD was lower in PKD2$^{-/-}$ than in WT T lymphoblasts (Figure 9, bottom). The lack of PKD2 thus reduced both AICD and CTL activity in primary T lymphoblasts.

Discussion

Exosomes are constitutively secreted by a variety of cell lineages and tumor cells, but T and B lymphocytes are the only cells in which triggering of antigen receptors (which regulate antigen-specific immune responses) controls inducible exosome secretion.[54, 55] T lymphocyte activation induces an increase in the number of mature MVB that contain ILV bearing membrane-bound FasL.[9] IS formation leads to polarization and membrane fusion of MVB, which release ILV as FasL-containing exosomes that trigger Fas-dependent AICD.[13, 33] CTL cytotoxic granules also have a MVB structure that stores perforin, granzymes and FasL[44] and release their content to the synaptic cleft as exosomes.[10] AICD maintains T lymphoid homeostasis,[56, 57] whereas CTL degranulation leads to specific, TCR-controlled target cell apoptosis.[55] MVB biogenesis and secretion are thus important for immune effector responses and T cell homeostasis.

DGKα acts as negative regulator of MVB maturation and exosome secretion by T lymphocytes,[9, 14] and might thus impair AICD by limiting the release of lethal, FasL-bearing exosomes. This DGKα role contrasts with its positive function in MVB polarization to the IS.[9] The molecular basis of this dual DGKα contribution to MVB formation and polarization is not fully understood, but might be linked to its ability to transform DAG into PA. Recent studies showed that DGKα controls late endosome polarized traffic in various cell lineages. DGKα-deficient CTL show defects in formation of the DAG gradient at the IS as well as MTOC (microtubule-organizing center) reorientation.[58] In breast carcinoma cells, DGKα-mediated PA generation mediates integrin recycling at the tips of invasive pseudopodial structures during invasive migration.[59] Additional studies are needed to determine whether DGKα-generated PA and/or its DAG consumption are necessary for MVB polarization to the IS.

Here we identify PKD as the major DAG effector that regulates MVB maturation and exosome secretion in T and B lymphocytes. Using pharmacological inhibition, DGKα overexpression and siRNA-mediated DGKα silencing, we show that DGKα controls MVB-mediated secretory traffic at least in part by limiting PKD activation. The effects of the R59949 DGK inhibitor are consistent with results for NIH3T3 cells, which showed that several growth factors that function via PLC can activate PKC at submaximal concentrations following DGK inhibition.[60] DGKα inhibition enhances exosome secretion in cells that express a PKD1 mutant that bypasses PKC activation requirements (GFP-PKD1CA); this suggests that in addition to limiting PKD phosphorylation by PKC, DGKα controls direct PKD activation by DAG.

The PKD effectors that contribute to regulation of MVB maturation are not known. The aberrant $CD63^+$ endosome phenotype in $PKD1^{-/-}3^{-/-}$ DT40 B cells resembles that observed after PI3K inhibition (Figure 6A). This suggests a role for PKD upstream of PI3K and correlates with recent studies that identified PKD phosphorylation and activation of class III PI3K Vps34 (ref. 61). PI3P is a master organizer of endosomal sorting, and promotes recruitment of several proteins that regulate various steps in trafficking, including endosomal fusion and ESCRT-dependent intraluminal sorting of cargoes.[62] J-HM1-2.2 cells that express an ATPase-deficient mutant VPS4 (ref. 9) have enlarged, ring-shaped endosomes similar to those seen in DT40 cells after PI3K inhibition. The comparable anomalous shape of $CD63^+$ vesicles in $PDK2^{-/-}$ cells suggests that PKD2 acts as a DAG sensor that also modulates membrane PI3P levels.

PKD2 is the major PKD isotype expressed in human and mouse T lymphocytes.[25, 26] In Jurkat T cells, GFP-tagged PKD1 and endogenous PKD2 have identical regulatory mechanisms, as well as similar activation kinetics and subcellular localization in response to TCR.[63] Here we show that a kinase-deficient PDK1 mutant with dominant negative

properties inhibits endogenous PDK, as indicated by lack of exosome secretion. The effects of the exogenously expressed GFP-PKD1CA mutant might be due to activation of PKD2 downstream effectors. The PKD2$^{-/-}$ mouse model confirms the contribution of this isoform to exosome secretion, and extends findings from DT40 B and Jurkat T cell lines to primary T lymphocytes. In response to TCR triggering, PKD2$^{-/-}$ T lymphoblasts show severe inhibition of IL-2 secretion,[26] although TCR-induced IL-2 gene expression was unaffected.[64] Defective IL-2 secretion by PKD2$^{-/-}$ T cells and the impaired exosome secretion we describe here could indicate a general secretion defect due to loss of PKD2. Indeed, a recent phosphoproteomic study of PKD2$^{-/-}$ CTL identified several traffic-related proteins as PKD2 substrates.[65]

Our data characterize a role for PKD2 in primary T cell AICD and coincide with studies showing that transient expression of a constitutively active PKD2 mutant in Jurkat cells enhances AICD.[25] Although loss of PKD2 enhances thymic output during T lymphocyte development, it does not affect T cell selection or inhibit expression of Vβ8 TCR,[64] the major murine TCR repertoire recognized by SEB.[50] After TCR activation of PKD2$^{-/-}$ T lymphoblasts, there is no change in the transcriptional induction of genes that encode proteins involved in CTL activity and AICD, such as FasL and perforin.[55, 64] It remains to be determined whether the splenomegaly and lymphadenopathy in TCR transgenic PKD2$^{-/-}$ mice are due exclusively to enhanced thymic output[64] or whether there is a contribution by an AICD defect in peripheral T lymphocytes. The decrease in CTL activity of PKD2$^{-/-}$versus WT T lymphoblasts-containing mixed cultures is underestimated, since PKD2$^{-/-}$ T lymphocytes undergo less AICD than WT T lymphoblasts (Figure 9), leading to an increase in the number of effector PKD2$^{-/-}$ T lymphoblasts. This reinforces the role of PKD2 as an important regulator of CTL activity.

Several studies have established an essential role for PKD and its activator DAG in Golgi-dependent secretory function. DAG-mediated PKD activation regulates vesicle budding and fission from the TGN, a process negatively regulated by DGK.[16, 19, 66] Our results here identify an additional PKD1/2 function as a major downstream effector of DGKα in the control of MVB traffic and exosome secretion in T and B cells. DGKα-mediated DAG consumption limits PKD subcellular location and activation in T ymphocytes during IS formation. PKD1/2 is necessary for MVB maturation and exosome secretion in T and some B cells, and thus contributes to crucial lymphocyte immune functions such as cytotoxic activity and AICD.

Materials and Methods

Cells and mice

J-HM1-2.2 Jurkat cells expressing human muscarinic type 1 receptor (HM1R)[67] were stimulated with carbachol (Sigma; final concentration 500 μM)[68] or plate-bound anti-CD3 antibody (10 μg/ml, UCHT1; BD Biosciences), or PMA (10 ng/ml) plus ionomycin (0.5 μg/ml). We used the DGK inhibitor II R59949 (10 μM; Calbiochem), the PKC inhibitor RO318220 (0.5 μM; Roche) and the PI3K inhibitor LY294002 (10 μM; Promega). The human Raji B cell and the EL-4 mouse T cell lines (ATCC) were used for immune synapse experiments. Generation, culture and activation of $PKD1^{-/-}3^{-/-}$ and $PKD1^{-/-}$ DT40 B cell lines were described.[36] Cells were stimulated with PMA/ionomycin or with mouse anti-chicken IgM (10 μg/ml, M4; Southern Biotech). C57BL/6 $PKD2^{-/-}$ mice and their WT littermates were bred and maintained in the Wellcome Trust Biocentre, University of Dundee (Scotland) in compliance with UK Home Office Animals (Scientific Procedures) Act 1986 guidelines. For activation of primary T cells, spleens were removed, mashed in cell strainers (Becton Dickinson), disaggregated, erythrocytes lysed, and the splenocytes suspended in RPMI 1640 medium containing L-glutamine (Invitrogen) with 10% heat-inactivated FCS (Gibco), penicillin/streptomycin (Gibco), and 50 μM β-mercaptoethanol (Sigma). Splenocytes were activated for 48 h with 1 μg/ml anti-CD3 antibody (2C11) to trigger the TCR. Following activation, cells were washed to remove 2C11 antibody and cultured (0.5×10^6 cells/ml) in medium supplemented with IL-2 (20 ng/ml).

Antibodies and reagents

We used anti-DGKα antibody (Abnova), anti-human TCR (UCHT1; BD Biosciences) and -mouse TCR (2C11; Santa Cruz). Polyclonal anti-PKD, -pPKD (S744/748) and -pPKD (S916) were from Cell Signaling. Rabbit polyclonal anti-FasL (CD95L; Q-20) was from Santa Cruz, anti-CD63 (NKI-C-3) from Oncogene and anti-lyso-bisphosphatidic acid

(LBPA; clone 6C4) from Echelon. Horseradish peroxidase-coupled secondary antibodies were from Dako. Carbachol (CCh) was from Sigma, annexin V-PE from Immunostep, and AlexaFluor-coupled secondary antibodies from Invitrogen. Staphylococcal enterotoxin E (SEE) and B (SEB) were from Toxin Technology and cell tracker blue (CMAC) from Invitrogen.

Expression vectors, transfection assays and retroviral transduction

pEFbos-GFP and pEFGFP-DGKα have been described;[14, 23] pEFGFP-C1-CD63 and pECFP-C1-CD63 were a generous gift from Dr. G. Griffiths;[69] pEFGFP-PKD1wt, pEFGFP-PKD1-D733A and pEFGFP-PKD1-S744E/S748E have been described.[27] pDsRed2-CD63 and pDsRed2-PKD1wt were prepared by subcloning cDNA for human CD63 from pEFGFP-C1-CD63, or PKD1wt from pEFGFP-C1-PKD1wt, into the pDsRed2-C1 vector (BD Biosciences). Constructs were verified by sequencing. Expression vectors for GFP-VPS4 wt and GFP-VPS4EQ mutant were a gift of Dr. P. Whitley.[70] For transfection experiments, J-HM1-2.2 or DT40 cells were transiently transfected with 20-30 μg of plasmids as described,[71] DGKα was silenced using the pSUPER RNAi System (pSR-GFP bicistronic or pSuper plasmids; Oligoengine) with the appropriate hairpin.[9]

The retroviral vector pBMN-Z (Addgene) was *HindIII*- and *NotI*-digested to remove *LacZ*; a 0.7-kb insert bearing EGFP (NCBI AAB02574.1) was excised from EGFP-N1 (Clontech) using *HindIII* and *NotI* and inserted into pBMN in place of *LacZ* (pBMN-GFP). PKD2wt cDNA was excised from pCR-Blunt II-TOPO-PKD2WT using *HindIII* and *NotI* and inserted into the digested pBMN vector (pBMN-GFP-PKD2). Human CD63 was excised from pCR-Blunt-EFGFP-CD63 using *NotI* and inserted into digested pBMN vector to yield pBMN-GFP-hCD63. Constructs were verified by sequencing. Phoenix ecotropic packaging cells (Stanford University) were transfected with 5-10 μg plasmid (pBMN-GFP, pBMN-GFP-CD63, pBMN-GFP-PKD2wt) using a standard calcium-phosphate transfection

protocol. At ~12-18 h post-transfection, medium renewed. After 24 h (37ºC, 5% CO_2), retroviral supernatants were centrifuged briefly (500 xg, 5 min) to remove packaging cells and viral particles concentrated by high-speed centrifugation (20,000 xg, 4 h, 4ºC). Supernatants were discarded and concentrated viral particles resuspended in 1 ml medium, snap-frozen and stored at -80ºC. Primary spleen T cells (10^6 cells/well) were mixed with freshly thawed retrovirus supernatant (1 ml) and polybrene (Sigma; 10 μg/ml). Plates were centrifuged (650 xg, 60 min), 1 ml/well IL-2-containing medium (20 ng/ml) was added and cells were incubated (24 h), then centrifuged to remove polybrene, resuspended in fresh medium with IL-2 and incubated as before. Infection efficiency was assessed at 48 h using epifluorescence microscopy to detect GFP^+ cells. We infected $PKD2^{-/-}$ T lymphoblasts with helper-free ecotropic and amphotropic retrovirus stock (with pBMN-EGFP-CD63) to obtain GFP-CD63-expressing cells; for GFP-PKD2 reconstitution experiments, we infected $PKD2^{-/-}$ T lymphoblasts with a mixed retrovirus stock (pBMN-EGFP-CD63 and pBMN-GFP-PKD2).

Isolation and quantitation of exosomes

Exosomes were isolated from culture supernatants as described.[32, 33, 34] There were no differences in β-actin levels in cell lysates, which indicates that the exosomes were produced by equal numbers of viable cells. Using standard protocols, supernatants of 20 x 10^6 cells were centrifuged sequentially at low speed, clarified,[72] and exosomes recovered by ultracentrifugation (100,000 xg, 12 h, 4ºC).[33] In experiments to quantify exosomes and analyze their size distribution, the final culture supernatant collected before ultracentrifugation was diluted (1/5) in HBSS and analyzed using NANOSIGHT (calibrated with 100 and 400 nm fluorescent calibration beads; Malvern). We analyzed exosomes from cells expressing the exosome reporters GFP-CD63 and DsRed2-CD63 in a similar protocol, using 10^6 J-HM1-2.2 cells or 4 x 10^6 DT40 cells. To measure endogenous CD63 in

exosomes, we normalized WB signals for exosome-producing cell number to those for β-actin or endogenous CD63. To analyze GFP-CD63 or DsRed2-CD63 reporters in exosomes, we normalized WB signals for exosome CD63 to those in cell lysates for each condition tested.

CD63 is found in MVB, ILV and hence in exosomes; this protein and its chimeras (GFP-CD63) are used as reporters for MVB/exosomes,[2, 8, 14], and allow quantitation of exosome secretion.[72, 9] Western blot analysis of endogenous or chimeric CD63 in isolated exosomes is used to measure exosomes[9], since the signal correlates with nanoparticle concentration data (nanoparticles/ml) as confirmed by Nanopaticle Tracking Analysis (NTA)[73, 74] (Supplementary Figure S2). In preliminary experiments, we probed WB of purified exosomes with another exosome marker (Lamp-1) and plasma membrane markers (CD45, CD28), to exclude the presence of cell debris, apoptotic bodies and/or shedding vesicles (Supplementary Figure S2). For murine T lymphoblasts, culture supernatants of 18 x 10^6 uninfected cells were concentrated (Amicon Ultra; Millipore) and centrifuged sequentially. Exosomes were obtained from 2 x 10^6 spleen T lymphoblasts expressing the exosome reporter GFP-CD63.

Preparation of whole cell and exosome lysates and Western blot analysis

Exosomes were resuspended in 60 μl RIPA lysis buffer and 20 μl of this lysate were analyzed by WB. We generally obtained 50-150 μg protein in the pellet from 20 x 10^6 stimulated cells. For WB, each lane contained the total exosomal protein recovered from medium for the same number of untreated or stimulated cells. Cells and exosomes were lysed (10 min) in RIPA buffer with protease inhibitors, proteins separated in reducing SDS-PAGE and transferred to Hybond ECL membranes (GE Healthcare). For CD63 detection, proteins were separated in non-reducing conditions.[75] Blots were incubated with rabbit anti-pPKD or mouse anti-CD63 and developed with appropriate HRP-conjugated secondary

antibodies using ECL reagents following standard protocols. Data were quantitated using Quantity One 4.4.0 software (Bio-Rad).

Immunofluorescence

Living cells expressing GFP-CD63 were attached to fibronectin-coated glass-bottom 35 mm culture dishes (Mat-Tek) at 24-48 h post-transfection, and stimulated in medium without phenol red (37ºC).[71] Immune synapses between transfected Jurkat cells and SEE-pulsed (1 μg/ml), CMAC-labeled Raji cells were analyzed as described[9]. In mouse cell immune synapse experiments, CMAC-labeled EL-4 cells were SEB-pulsed (1 μg/ml) and challenged with T lymphoblasts from WT mice at a 1:1 ratio. For time-lapse video experiments, we using an OKO-lab stage incubator on a Nikon Eclipse TiE microscope with a DS-Qi1MC digital camera and a Plan Apo VC 60x NA 1.4 objective. For video acquisition and analysis, we used NIS-AR software (Nikon). Epifluorescence images were deconvoluted with Huygens Deconvolution Software (Scientific Volume Image). Digital images were quantified with NIS-AR or ImageJ software (Rasband, WS, ImageJ, US National Institutes of Health, , http://rsb.info.nih.gov/ij/). Video images of GFP-CD63 vesicle trajectories were plotted and analyzed with NIS-AR and ImageJ MJTrack plugin. Significance of results for single cells was determined using ANOVA to analyze at least 20 cells from different fields for at least three experiments per condition.

CTL and AICD assays

For CTL and AICD assays, EL-4 cells were SEB-pulsed (1 μg/ml) and challenged with WT and PKD2$^{-/-}$ mouse T lymphoblasts at various effector/target ratios in U-bottom 96-well culture plates (5 h), then annexinV-PE-stained to analyze the percentage of apoptotic cells by flow cytometry. Forward and side scatter detectors were calibrated to optimize discrimination of the cell populations, to gate EL-4 and T lymphoblasts by size and

complexity, and simultaneously measure percentage of apoptosis of EL-4 (CTL activity) and T lymphoblasts (AICD).

Acknowledgements

We are indebted to Doreen Cantrell (University of Dundee, UK) for her generous and continuous support, reagents and superb advice. We acknowledge Elizabeth Emslie and Maria Navarro for their help and comments, Mark Ware (Nanosight Ltd, UK) for his support in NANOSIGHT studies, and Catherine Mark for excellent editorial assistance. The authors have no conflicting financial interests.

RA received a doctoral fellowship from the Spanish Ministerio de Ciencia y Tecnología. This work was supported by grants from the Spanish Ministerio de Economía y Competitividad (MINECO) Plan Nacional de Investigación Científica (BFU2011-22849 to MI). IM is funded by MINECO grant BFU2013-47640-P.

Supplementary information is available at Cell Death and Differentiation website.

References

1. Lakkaraju A, Rodriguez-Boulan E. Itinerant exosomes: emerging roles in cell and tissue polarity. *Trends Cell Biol* 2008; **18:** 199-209.
2. Raiborg C, Rusten TE, Stenmark H. Protein sorting into multivesicular endosomes. *Curr Opin Cell Biol* 2003, **15**(4)**:** 446-455.
3. Thery C, Zitvogel L, Amigorena S. Exosomes: composition, biogenesis and function. *Nat Rev Immunol* 2002, **2**(8)**:** 569-579.
4. Marsh M, van Meer G. Cell biology. No ESCRTs for exosomes. *Science* 2008, **319:** 1191-1192.
5. Babst M. MVB vesicle formation: ESCRT-dependent, ESCRT-independent and everything in between. *Curr Opin Cell Biol* 2011.
6. Williams RL, Urbe S. The emerging shape of the ESCRT machinery. *Nat Rev Mol Cell Biol* 2007, **8**(5)**:** 355-368.
7. Matsuo H, Chevallier J, Mayran N, Le Blanc I, Ferguson C, Faure J*, et al.* Role of LBPA and Alix in multivesicular liposome formation and endosome organization. *Science* 2004, **303**(5657)**:** 531-534.
8. Trajkovic K, Hsu C, Chiantia S, Rajendran L, Wenzel D, Wieland F*, et al.* Ceramide triggers budding of exosome vesicles into multivesicular endosomes. *Science* 2008, **319**(5867)**:** 1244-1247.
9. Alonso R, Mazzeo C, Rodriguez MC, Marsh M, Fraile-Ramos A, Calvo V*, et al.* Diacylglycerol kinase alpha regulates the formation and polarisation of mature multivesicular bodies involved in the secretion of Fas ligand-containing exosomes in T lymphocytes. *Cell Death Differ* 2011, **18**(7)**:** 1161-1173.
10. Peters PJ, Geuze HJ, Van der Donk HA, Slot JW, Griffith JM, Stam NJ*, et al.* Molecules relevant for T cell-target cell interaction are present in cytolytic granules of human T lymphocytes. *Eur J Immunol* 1989, **19**(8)**:** 1469-1475.
11. Stoorvogel W, Kleijmeer MJ, Geuze HJ, Raposo G. The biogenesis and functions of exosomes. *Traffic* 2002, **3**(5)**:** 321-330.
12. Zuccato E, Blott EJ, Holt O, Sigismund S, Shaw M, Bossi G*, et al.* Sorting of Fas ligand to secretory lysosomes is regulated by mono-ubiquitylation and phosphorylation. *J Cell Sci* 2007, **120**(Pt 1)**:** 191-199.
13. Monleon I, Martinez-Lorenzo MJ, Monteagudo L, Lasierra P, Taules M, Iturralde M*, et al.* Differential secretion of Fas ligand- or APO2 ligand/TNF-related apoptosis-inducing ligand-carrying microvesicles during activation-induced death of human T cells. *J Immunol* 2001, **167**(12)**:** 6736-6744.
14. Alonso R, Rodriguez MC, Pindado J, Merino E, Merida I, Izquierdo M. Diacylglycerol kinase alpha regulates the secretion of lethal exosomes bearing Fas ligand during activation-induced cell death of T lymphocytes. *J Biol Chem* 2005, **280**(31)**:** 28439-28450.
15. Mittelbrunn M, Gutierrez-Vazquez C, Villarroya-Beltri C, Gonzalez S, Sanchez-Cabo F, Gonzalez MA*, et al.* Unidirectional transfer of microRNA-loaded exosomes from T cells to antigen-presenting cells. *Nature communications* 2011, **2:** 282.
16. Litvak V, Dahan N, Ramachandran S, Sabanay H, Lev S. Maintenance of the diacylglycerol level in the Golgi apparatus by the Nir2 protein is critical for Golgi secretory function. *Nat Cell Biol* 2005, **7**(3)**:** 225-234.
17. Roth MG. Lipid regulators of membrane traffic through the Golgi complex. *Trends Cell Biol* 1999, **9**(5)**:** 174-179.
18. Sprong H, van der Sluijs P, van Meer G. How proteins move lipids and lipids move proteins. *Nat Rev Mol Cell Biol* 2001, **2**(7)**:** 504-513.
19. Baron CL, Malhotra V. Role of diacylglycerol in PKD recruitment to the TGN and protein transport to the plasma membrane. *Science* 2002, **295**(5553)**:** 325-328.
20. Quann EJ, Merino E, Furuta T, Huse M. Localized diacylglycerol drives the polarization of the microtubule-organizing center in T cells. *Nat Immunol* 2009, **10**(6)**:** 627-635.
21. Van Lint J, Rykx A, Maeda Y, Vantus T, Sturany S, Malhotra V*, et al.* Protein kinase D: an intracellular traffic regulator on the move. *Trends Cell Biol* 2002, **12**(4)**:** 193-200.

22. Merida I, Avila-Flores A, Merino E. Diacylglycerol kinases: at the hub of cell signalling. *Biochem J* 2008, **409**(1)**:** 1-18.
23. Sanjuan MA, Jones DR, Izquierdo M, Merida I. Role of diacylglycerol kinase alpha in the attenuation of receptor signaling. *J Cell Biol* 2001, **153**(1)**:** 207-220.
24. Sanjuan MA, Pradet-Balade B, Jones DR, Martinez AC, Stone JC, Garcia-Sanz JA*, et al.* T cell activation in vivo targets diacylglycerol kinase alpha to the membrane: a novel mechanism for Ras attenuation. *J Immunol* 2003, **170**(6)**:** 2877-2883.
25. Irie A, Harada K, Tsukamoto H, Kim JR, Araki N, Nishimura Y. Protein kinase D2 contributes to either IL-2 promoter regulation or induction of cell death upon TCR stimulation depending on its activity in Jurkat cells. *Int Immunol* 2006, **18**(12)**:** 1737-1747.
26. Matthews SA, Navarro MN, Sinclair LV, Emslie E, Feijoo-Carnero C, Cantrell DA. Unique functions for protein kinase D1 and protein kinase D2 in mammalian cells. *Biochem J* 2010, **432**(1)**:** 153-163.
27. Matthews SA, Rozengurt E, Cantrell D. Characterization of serine 916 as an in vivo autophosphorylation site for protein kinase D/Protein kinase Cmu. *J Biol Chem* 1999, **274**(37)**:** 26543-26549.
28. Alonso R, Mazzeo C, Merida I, Izquierdo M. A new role of diacylglycerol kinase alpha on the secretion of lethal exosomes bearing Fas ligand during activation-induced cell death of T lymphocytes. *Biochimie* 2007, **89**(2)**:** 213-221.
29. Matthews SA, Rozengurt E, Cantrell D. Protein kinase D. A selective target for antigen receptors and a downstream target for protein kinase C in lymphocytes. *J Exp Med* 2000, **191**(12)**:** 2075-2082.
30. Waldron RT, Rey O, Iglesias T, Tugal T, Cantrell D, Rozengurt E. Activation loop Ser744 and Ser748 in protein kinase D are transphosphorylated in vivo. *J Biol Chem* 2001, **276**(35)**:** 32606-32615.
31. Iglesias T, Waldron RT, Rozengurt E. Identification of in vivo phosphorylation sites required for protein kinase D activation. *J Biol Chem* 1998, **273**(42)**:** 27662-27667.
32. Blanchard N, Lankar D, Faure F, Regnault A, Dumont C, Raposo G*, et al.* TCR activation of human T cells induces the production of exosomes bearing the TCR/CD3/zeta complex. *J Immunol* 2002, **168**(7)**:** 3235-3241.
33. Martinez-Lorenzo MJ, Anel A, Gamen S, Monle n I, Lasierra P, Larrad L*, et al.* Activated human T cells release bioactive Fas ligand and APO2 ligand in microvesicles. *J Immunol* 1999, **163**(3)**:** 1274-1281.
34. Andreola G, Rivoltini L, Castelli C, Huber V, Perego P, Deho P*, et al.* Induction of lymphocyte apoptosis by tumor cell secretion of FasL-bearing microvesicles. *J Exp Med* 2002, **195**(10)**:** 1303-1316.
35. Montoya MC, Sancho D, Bonello G, Collette Y, Langlet C, He HT*, et al.* Role of ICAM-3 in the initial interaction of T lymphocytes and APCs. *Nat Immunol* 2002, **3**(2)**:** 159-168.
36. Matthews SA, Liu P, Spitaler M, Olson EN, McKinsey TA, Cantrell DA*, et al.* Essential role for protein kinase D family kinases in the regulation of class II histone deacetylases in B lymphocytes. *Mol Cell Biol* 2006, **26**(4)**:** 1569-1577.
37. Muntasell A, Berger AC, Roche PA. T cell-induced secretion of MHC class II-peptide complexes on B cell exosomes. *EMBO J* 2007, **26**(19)**:** 4263-4272.
38. Arita S, Baba E, Shibata Y, Niiro H, Shimoda S, Isobe T*, et al.* B cell activation regulates exosomal HLA production. *Eur J Immunol* 2008, **38**(5)**:** 1423-1434.
39. Raposo G, Nijman HW, Stoorvogel W, Liejendekker R, Harding CV, Melief CJ*, et al.* B lymphocytes secrete antigen-presenting vesicles. *J Exp Med* 1996, **183**(3)**:** 1161-1172.
40. Wubbolts R, Leckie RS, Veenhuizen PT, Schwarzmann G, Mobius W, Hoernschemeyer J*, et al.* Proteomic and biochemical analyses of human B cell-derived exosomes. Potential implications for their function and multivesicular body formation. *J Biol Chem* 2003, **278**(13)**:** 10963-10972.
41. Liu P, Scharenberg AM, Cantrell DA, Matthews SA. Protein kinase D enzymes are dispensable for proliferation, survival and antigen receptor-regulated NFkappaB activity in vertebrate B-cells. *FEBS Lett* 2007, **581**(7)**:** 1377-1382.

42. Rous BA, Reaves BJ, Ihrke G, Briggs JA, Gray SR, Stephens DJ*, et al.* Role of adaptor complex AP-3 in targeting wild-type and mutated CD63 to lysosomes. *Mol Biol Cell* 2002, **13**(3)**:** 1071-1082.
43. Bossi G, Griffiths GM. Degranulation plays an essential part in regulating cell surface expression of Fas ligand in T cells and natural killer cells. *Nat Med* 1999, **5**(1)**:** 90-96.
44. Stinchcombe JC, Griffiths GM. Regulated secretion from hemopoietic cells. *J Cell Biol* 1999, **147**(1)**:** 1-6.
45. Fernandez-Borja M, Wubbolts R, Calafat J, Janssen H, Divecha N, Dusseljee S*, et al.* Multivesicular body morphogenesis requires phosphatidyl-inositol 3-kinase activity. *Curr Biol* 1999, **9**(1)**:** 55-58.
46. Granboulan M, Lankar D, Raposo G, Bonnerot C, Hivroz C. Phosphoinositide 3-kinase activation by Igbeta controls de novo formation of an antigen-processing compartment. *J Biol Chem* 2003, **278**(6)**:** 4331-4338.
47. Futter CE, Collinson LM, Backer JM, Hopkins CR. Human VPS34 is required for internal vesicle formation within multivesicular endosomes. *J Cell Biol* 2001, **155**(7)**:** 1251-1264.
48. Reaves BJ, Bright NA, Mullock BM, Luzio JP. The effect of wortmannin on the localisation of lysosomal type I integral membrane glycoproteins suggests a role for phosphoinositide 3-kinase activity in regulating membrane traffic late in the endocytic pathway. *J Cell Sci* 1996, **109 (Pt 4):** 749-762.
49. Odorizzi G, Babst M, Emr SD. Phosphoinositide signaling and the regulation of membrane trafficking in yeast. *Trends Biochem Sci* 2000, **25**(5)**:** 229-235.
50. White J, Herman A, Pullen AM, Kubo R, Kappler JW, Marrack P. The V beta-specific superantigen staphylococcal enterotoxin B: stimulation of mature T cells and clonal deletion in neonatal mice. *Cell* 1989, **56**(1)**:** 27-35.
51. Izquierdo M, Grandien A, Criado ML, Robles S, Leonardo E, Albar JP*, et al.* Blocked negative selection of developing T cells in mice expressing the baculovirus p35 caspase inhibitor. *EMBO J* 1999, **18:** 101-111.
52. Morales-Kastresana A, Catalán E, Hervás-Stubbs S, Palazón A, Azpilikueta A, Bolaños E*, et al.* Essential complicity of perforin-granzyme and FAS-L mechanisms to achieve tumor rejection following treatment with anti-CD137 mAb. *Journal for ImmunoTherapy of Cancer* 2013, **1**(3).
53. Pardo J, Bosque A, Brehm R, Wallich R, Naval J, Mullbacher A*, et al.* Apoptotic pathways are selectively activated by granzyme A and/or granzyme B in CTL-mediated target cell lysis. *J Cell Biol* 2004, **167**(3)**:** 457-468.
54. Thery C, Ostrowski M, Segura E. Membrane vesicles as conveyors of immune responses. *Nat Rev Immunol* 2009, **9**(8)**:** 581-593.
55. de Saint Basile G, Menasche G, Fischer A. Molecular mechanisms of biogenesis and exocytosis of cytotoxic granules. *Nat Rev Immunol* 2010, **10**(8)**:** 568-579.
56. Nagata S, Suda T. Fas and Fas ligand: lpr and gld mutations. *Immunol Today* 1995, **16**(1)**:** 39-43.
57. Krammer PH, Arnold R, Lavrik IN. Life and death in peripheral T cells. *Nat Rev Immunol* 2007, **7**(7)**:** 532-542.
58. Chauveau A, Le Floc'h A, Bantilan NS, Koretzky GA, Huse M. Diacylglycerol kinase alpha establishes T cell polarity by shaping diacylglycerol accumulation at the immunological synapse. *Sci Signal* 2014, **7**(340)**:** ra82.
59. Rainero E, Caswell PT, Muller PA, Grindlay J, McCaffrey MW, Zhang Q*, et al.* Diacylglycerol kinase alpha controls RCP-dependent integrin trafficking to promote invasive migration. *J Cell Biol* 2012, **196**(2)**:** 277-295.
60. Zugaza JL, Waldron RT, Sinnett-Smith J, Rozengurt E. Bombesin, vasopressin, endothelin, bradykinin, and platelet-derived growth factor rapidly activate protein kinase D through a protein kinase C-dependent signal transduction pathway. *J Biol Chem* 1997, **272**(38)**:** 23952-23960.
61. Eisenberg-Lerner A, Kimchi A. PKD is a kinase of Vps34 that mediates ROS-induced autophagy downstream of DAPk. *Cell Death Differ* 2012, **19**(5)**:** 788-797.
62. Morel E, Chamoun Z, Lasiecka ZM, Chan RB, Williamson RL, Vetanovetz C*, et al.* Phosphatidylinositol-3-phosphate regulates sorting and processing of amyloid precursor protein through the endosomal system. *Nature communications* 2013, **4:** 2250.

63. Spitaler M, Emslie E, Wood CD, Cantrell D. Diacylglycerol and protein kinase D localization during T lymphocyte activation. *Immunity* 2006, **24**(5)**:** 535-546.
64. Navarro MN, Sinclair LV, Feijoo-Carnero C, Clarke R, Matthews SA, Cantrell DA. Protein kinase D2 has a restricted but critical role in T-cell antigen receptor signalling in mature T-cells. *Biochem J* 2012, **442**(3)**:** 649-659.
65. Navarro MN, Goebel J, Hukelmann JL, Cantrell DA. Quantitative phosphoproteomics of cytotoxic T cells to reveal protein kinase d 2 regulated networks. *Mol Cell Proteomics* 2014, **13**(12)**:** 3544-3557.
66. Ghanekar Y, Lowe M. Signalling for secretion. *Nat Cell Biol* 2005, **7**(9)**:** 851-853.
67. Desai DM, Newton ME, Kadlecek T, Weiss A. Stimulation of the phosphatidylinositol pathway can induce T cell activation. *Nature* 1990, **348:** 66-69.
68. Izquierdo M, Ruiz-Ruiz MC, López-Rivas A. Stimulation of the PtdIns turnover is a key event for Fas-dependent, activation-induced apoptosis in human T lymphocytes. *J Immunol* 1996, **157:** 21-28.
69. Blott EJ, Bossi G, Clark R, Zvelebil M, Griffiths GM. Fas ligand is targeted to secretory lysosomes via a proline-rich domain in its cytoplasmic tail. *J Cell Sci* 2001, **114**(Pt 13)**:** 2405-2416.
70. Whitley P, Reaves BJ, Hashimoto M, Riley AM, Potter BV, Holman GD. Identification of mammalian Vps24p as an effector of phosphatidylinositol 3,5-bisphosphate-dependent endosome compartmentalization. *J Biol Chem* 2003, **278**(40)**:** 38786-38795.
71. Jambrina E, Alonso R, Alcalde M, Rodríguez MC, Serrano A, Martínez-A. C*, et al.* Calcium influx through receptor-operated channel induces mitochondria-triggered paraptotic cell death. *J BiolChem* 2003, **278:** 14134-14145.
72. Thery C, Amigorena S, Raposo G, Clayton A. Isolation and characterization of exosomes from cell culture supernatants and biological fluids. *Curr Protoc Cell Biol* 2006, **Chapter 3:** Unit 3 22.
73. Dragovic RA, Gardiner C, Brooks AS, Tannetta DS, Ferguson DJ, Hole P*, et al.* Sizing and phenotyping of cellular vesicles using Nanoparticle Tracking Analysis. *Nanomedicine* 2011, **7**(6)**:** 780-788.
74. Soo CY, Song Y, Zheng Y, Campbell EC, Riches AC, Gunn-Moore F*, et al.* Nanoparticle tracking analysis monitors microvesicle and exosome secretion from immune cells. *Immunology* 2012.
75. Wang R, Dworak LJ, Lacy MJ. A panel immunoblot using co-incubated monoclonal antibodies for identification of melanoma cells. *J Immunol Methods* 2001, **249**(1-2)**:** 167-183.

Figure legends

Fig. 1. PKC regulates exosome secretion. A) J-HM1-2.2 cells, alone or preincubated with RO318220, were stimulated with carbachol (CCh, 500 μM) or plate-bound anti-TCR mAb (UCHT1, 10 μg/ml) for 8 h to induce exosome secretion. Exosomes were isolated by sequential centrifugation. WB of exosome protein extracts were developed with anti-CD63, whereas WB of whole cell lysates were developed with β-actin antibody to normalize to cell number. In the left panel, whole cell lysates of PMA-treated J-HM1-2.2 cells are shown as a reference for CD63. B) Whole J-HM1-2.2 and exosome lysates in A) were analyzed with anti-FasL. In the left side lanes, whole cell lysates were run as a reference for FasL. C) Top table; quantification of WB signal shown in A) (mean arbitrary units; AU) in parallel with NANOSIGHT data (mean particles/ml) for the same samples. Bottom, mean *x*-fold induction data are shown for CD63 in exosomes (WB) and exosome concentration (NANOSIGHT). SD was <5% of the mean in all cases; * not significant (NS); ** $p \leq 0.05$.

Fig. 2. PKD regulates exosome secretion. A) J-HM1-2.2 cells were cotransfected with DsRed2-CD63 and the constructs GFP-PKD1 WT, GFP-PKD1 KD (kinase-dead) or GFP-PKD1CA (constitutively active). Cells were preincubated alone or with R59949 (R59, 10 μM) and stimulated with CCh (500 μM) to induce exosome secretion. Top, WB of exosome protein extracts developed with anti-CD63. For simplicity, R59949 alone was not included in these experiments; the inhibitor alone had no detectable effect on exosome secretion.[9, 14] Bottom, lysates of exosome-secreting cells were developed with anti-β-actin and -CD63 for normalization. B) Quantitation of results from three experiments similar to that in A). Exosome secretion by cells expressing the distinct constructs is expressed as *x*-fold induction (mean ± SD) of three experiments, normalized to cell DsRed2-CD63 levels. C) DsRed2-CD63-transfected J-HM1-2.2 cells, human T lymphoblasts, or human PBL, alone or R59949-treated, were stimulated as indicated to induce exosome secretion. Normalized

x-fold induction of exosome secretion was determined by WB analyses of DsRed2-CD63 and endogenous CD63 (eCD63). Inset, mean exosome concentration (particles/ml) secreted by the distinct cell types was determined by NANOSIGHT analyses; mean *x*-fold induction of exosome secretion is shown in brackets. SD was <5% of the mean in all cases; * NS; ** $p \leq 0.05$.

Fig. 3. GFP-PKD1 CA mutant expression enhances polarized exosome secretion. A) GFP-CD63-expressing Jurkat cells were challenged (2 h) with SEE-pulsed (1 μg/ml), CMAC-labeled Raji cells (blue) to induce formation of synaptic conjugates (S, synapse) and MVB polarization towards the immune synapse. Transmittance plus CMAC (blue; left panel), GFP-CD63 channel (center) and trajectories followed by GFP-CD63 vesicles (right) are shown (see also Supplementary Video 2). B) Jurkat cells that coexpressed GFP-CD63 and GFP or GFP-PKD1CA were challenged with SEE-pulsed Raji cells; exosomes were isolated, quantitated by WB analysis of the GFP-CD63 reporter and normalized for cell number and cellular GFP-CD63 content. Exosome secretion is expressed as *x*-fold induction (mean ± SD) of 3 independent experiments. ** $p \leq 0.05$.

Fig. 4. Exosome secretion in DT40 B lymphocytes. WT, $PKD1^{-/-}3^{-/-}$ and $PKD1^{-/-}$ DT40 cells ($PKD1^{-/-}3^{-/-}$ DT40 cells cultured with tetracycline to induce Flag-PKD3 expression; see Supplementary Fig. S3) were transfected with GFP-CD63 and stimulated for the indicated times with PMA (10 ng/ml) plus ionomycin (0.5 μg/ml) (A) or anti-IgM (10 μg/ml) (B). We analyzed GFP-CD63 in cell lysates and exosomes using WB and quantified the *x*-fold induction (mean ± SD) of exosome secretion of GFP-CD63, normalized to cell GFP-CD63 levels (C). Statistical significance corresponds to exosome secretion at the same time points of WT versus $PKD1^{-/-}3^{-/-}$ or $PKD1^{-/-}$ DT40 cells. In D), WT and $PKD1^{-/-}$ DT40 cells were stimulated with anti-IgM, exosomes isolated, and endogenous CD63 (eCD63) analyzed in cell lysates and exosomes using WB; quantification is shown in E), normalized to cellular

eCD63. Statistical significance corresponds to exosome secretion at the same time points of WT versus PKD1$^{-/-}$ DT40 cells. F) WT, PKD1$^{-/-}$3$^{-/-}$ DT40 cells and GFP-PKD1-transfected PKD1$^{-/-}$3$^{-/-}$ DT40 cells (PKD3$^{-/-}$ DT40 cells), all of which expressed GFP-CD63, were anti-IgM-stimulated and exosome secretion analyzed as above. Statistical significance corresponds to exosome secretion at the same time points of WT versus PKD3$^{-/-}$ DT40 cells. * NS; ** $p \leq 0.05$.

Fig. 5. MVB secretory traffic and exosome secretion in PKD2$^{-/-}$ T lymphoblasts. GFP-CD63-transduced WT or PKD2$^{-/-}$ T lymphoblasts were stimulated with plate-bound anti-TCR (α-TCR, 2C11, 10 μg/ml; 6 h) to induce MVB degranulation and exosome secretion. A) Top, quantitation of the GFP-CD63 fluorescence ratio (plasma membrane:total fluorescence) in WT and PKD2$^{-/-}$T lymphoblasts. Bottom, representative epifluorescence images of unstimulated or stimulated cells. B) WB analysis of cell PKD2 expression (left); WB analysis of exosome GFP-CD63 levels (right). C) PKD2$^{-/-}$ and GFP-PKD2-transduced PKD2$^{-/-}$ T lymphoblasts, both transduced with GFP-CD63, were anti-TCR stimulated as in A) and exosome secretion compared to that for WT T lymphoblasts. Results are quantified as *x*-fold induction (mean ± SD) of exosome secretion of GFP-CD63, normalized to cell GFP-CD63 levels. * NS; ** $p \leq 0.05$.

Fig. 6. PKDs control MVB maturation. A) WT and PKD1$^{-/-}$3$^{-/-}$ DT40 cells were transfected with GFP-CD63 and treated with PI3K inhibitor (LY294002, 10 μM; 4 h). GFP-CD63 fluorescence was imaged by epifluorescence and definition improved by deconvolution. B) GFP-CD63-transduced WT or PKD2$^{-/-}$ T lymphoblasts were stimulated with plate-bound anti-TCR (2C11, 10 μg/ml, 4 h) to induce MVB degranulation and GFP-CD63 relocalization to the plasma membrane and imaged by epifluorescence.

Fig. 7. DGKα regulates PKD1/2 phosphorylation. A) J-HM1-2.2 cells, alone or pretreated with DGK inhibitor II (R59949; 10 μM), were stimulated for the indicated times

with anti-TCR (10 μg/ml), anti-TCR plus anti-CD28 (10 μg/ml), or CCh (500 μM). WB of whole cell lysates was developed with the indicated antibodies to measure phosphorylation of the PKD1/2 (pSer 744/748) activation loop. B) J-HM1-2.2 cells were transfected with DsRed2-PKD1 alone (-) or cotransfected with GFP-DGKα (+), then stimulated with CCh (500 μM) or PMA (10 ng/ml) plus ionomycin (0.5 μg/ml) for times indicated. Cell lysates were analyzed by WB as above to determine phosphorylation of endogenous PKD1/PKD2 and DsRed2-PKD1 activation loops. * NS; ** $p \leq 0.05$.

Fig. 8. Interference with DGKα expression regulates PKD1/2 phosphorylation. A) Co-cultured Jurkat and CMAC-labeled Raji cells were untreated (Control) or stimulated with SEE (1 μg/ml) or PMA (10 ng/ml) (5 h). Confocal immunofluorescence images show phosphorylation of endogenous PKD1/2 (pSer916, red; top row), CD63 (green; second row), CMAC (Raji cells, blue; third row); bottom row shows merged images (yellow); S, synaptic contact. B) Jurkat cells transfected with a GFP-containing bicistronic interference plasmid for human DGKα were stimulated with SEE-pulsed, CMAC (blue)-labeled Raji cells (5 h) to induce synapse formation. Top row, representative immunofluorescence analysis showing GFP^+ Jurkat (green) and $CMAC^+$ Raji (blue) cells. Interference with DGKα expression was assessed by intracellular staining of endogenous DGKα (orange; second row). Third row, pSer916 phosphorylation of endogenous PKD1/2 was assessed using anti-pPKD1 (pSer916, red) antibody in GFP^+ ($DGK\alpha^-$; green arrow) and GFP^- ($DGK\alpha^+$; white arrow) Jurkat cells forming synaptic conjugates. Bottom row, red fluorescence channel (pPKD1/2) signal-to-noise ratio was improved using deconvolution. The transmittance panel is also included to show two synaptic conjugates formed by Jurkat (yellow contour) and Raji (light blue contour) cells. The arrows indicate the synaptic contact areas. Bottom panel, analysis of mean fluorescence intensity distribution for pSer916 PKD1/2 in synapse-forming $DGK\alpha^+$ and $DGK\alpha^-$ Jurkat cells; results from four experiments (with at least 100 synapse-forming

cells/condition) as in upper panels. Inset, MFI (mean ± SD) for active PKD in both cell populations. ** $p \leq 0.05$.

Fig. 9. PKD2 regulates CTL activity and AICD. Top, WT and PKD2$^{-/-}$ T lymphoblasts were challenged at the indicated cell:cell ratios with SEB-pulsed EL-4 cells (1 μg/ml; 6 h) Apoptosis was assessed in EL-4 cells (cytotoxicity) or T lymphoblasts (AICD) with annexinV-PE by flow cytometry. Results are expressed as the percentage of apoptotic cells. Bottom, AICD was analyzed as above for WT and PKD2$^{-/-}$ T lymphoblasts stimulated with plate-bound anti-TCR (2C11, 10 μg/ml). Statistical significance corresponds to percent of apoptosis of EL-4 and T lymphocytes at the same effector to target/stimulator cell ratio of WT versus PKD2 KO T lymphoblasts. ** $p \leq 0.05$.

Supplementary Material

Supplementary Fig. S1. RO318220 inhibits PKD1/2 phosphorylation. A) J-HM1-2.2 cells expressing GFP-PKD1WT or GFP-PKD1KD alone or preincubated with the PKC inhibitor RO318220 (0.5 μM), after which cells were PMA-stimulated (10 ng/ml; 1 h). Protein extracts from these cells were analyzed by WB with anti-pPKD1/2 (pSer 744/748) and reprobed with anti-GFP or -PKD1/2. B) J-HM1-2.2 cells untransfected or expressing GFP-PKD1 WT were pre-incubated with the PKC inhibitor RO318220 (0.5 μM) and stimulated with PMA (10 ng/ml, 1 h) or CCh (500 μM, 15 min and 6 h). Autophosphorylation of GFP-PKD1 and endogenous PKD1/2 was determined by WB analysis with anti-pPKD1/2 (pSer 916) and reprobed with anti-PKD1/2 as control.

Supplementary Fig. S2. Quantification of exosome secretion by NANOSIGHT analysis compared to WB analysis of isolated exosomes. A) Clarified culture supernatants of J-HM1-2.2 cells, alone or CCh-treated (50 μM), were analyzed with NANOSIGHT LM-10 calibrated with 100, 200 and 400 nm beads. Results show particle size distribution profiles and concentration (particles/ml) of the events between the two markers (50-150 nm). Particle size (mean ± SD) for control, 123 ± 52 nm and CCh, 133 ± 66. B) Exosomes were isolated from equal numbers of J-HM1-2.2 cells, alone or CCh-stimulated (50 or 500 μM). WB of exosomes was developed with two exosome (CD63, Lamp-1) and two plasma membrane markers (CD45, CD28). C) CD63 signal in WB in B) was quantitated with ImageJ and plotted against exosome concentration of the same samples assessed by NANOSIGHT. D) Results as in C), with data expressed as *x*-fold induction (mean ± SD). * NS.

Supplementary Fig. S3. Expression of inducible, functional Flag-PKD3 in DT40 cells. Top, DT40 WT and PKD1$^{-/-}$3$^{-/-}$ cells (bearing a doxycycline-inducible Flag-PKD3 expression construct) were cultured with tetracycline (Tet; ++, 10 μg/ml; + 1 μg/ml) to

induce Flag-PKD3 expression. WB was probed with anti-Flag to assess inducible Flag-PKD3 expression. Center, in a similar experiment, the WB was probed with anti-PKD3 antibody. Bottom, DT40 WT cells and PKD1$^{-/-}$3$^{-/-}$ as above were cultured with Tet as above, alone or treated with PMA (10 ng/ml, 1 h). Phosphorylation of PKD1 and PKD3 activation loops were analyzed by WB with anti-pPKD1/2 (pSer 744/748). β-actin was used as control.

Supplementary Fig. S4. MVB trajectories in TCR-stimulated T lymphoblasts. Fluorescence intensity on the four trajectories tracked in Supplementary Video 5. Red arrow, frame in which vesicles nº 1 and 2 reached the plasma membrane. Their docking at the plasma membrane was followed by a transient increase in fluorescence. These changes were not observed in trajectories of vesicles nº 3 and 4, which did not approach the plasma membrane. These data are compatible with fusion of vesicles nº 1 and 2 to the membrane. Fluorescence data along trajectories was obtained with the MJtrack ImageJ plug-in.

Supplementary Fig. S5. PKD1 half-life at the synapse in DGKα-silenced cells. Jurkat T lymphocytes were cotransfected with DsRed2-PKD1 and pSR-GFP or pSR-GFP siRNA-DGKα bicistronic plasmid. Control and DGKα-silenced were challenged with SEE-loaded, CMAC-labeled Raji cells, and time-lapse videos recorded (see Supplementary Video 7). Measurement of DsRed2-PKD1 fluorescence intensity changes were analyzed with NIS-AR software using an appropriate region of interest (ROI) at the synaptic area. Half-life of fluorescence decay (mean ± SD) at the synapse is shown for DGKα^{+} and DGKα^{-} cells. ** $p \leq 0.05$.

Supplementary Video 1. CMAC-labeled Raji cells (blue) were attached to fibronectin-coated MatTek chamber slides and SEE-pulsed (30 min). Double synapse formation by one GFP-CD63-expressing Jurkat cell was time-lapse imaged (right side). The video shows

MVB traffic to the synapse contact areas in this cell and not in Jurkat cells that do not form synapses (left). One representative example is shown of 11 synapses recorded.

Supplementary Video 2. GFP-CD63-transfected Jurkat cells were challenged with SEE-pulsed (1 μg/ml), CMAC-labeled Raji cells (blue) to induce synapse formation. The video shows the synapse imaged in Fig. 3A (middle) and the trajectories followed by GFP-CD63 vesicles (right). Videos for the GFP-CD63 channel were captured (7 frames/sec); a representative example is shown of 21 synapses recorded.

Supplementary Video 3. GFP-CD63-transduced WT mouse T lymphoblasts were cultured in fibronectin-coated IBIDI chamber slides to image MVB (GFP-CD63$^+$) traffic in unstimulated cells. Video time-lapse experiments (5 frames/sec) showed random movement of several intracellular GFP-CD63$^+$ vesicles and weak cell surface staining due to basal traffic and vesicle fusion to the plasma membrane.

Supplementary Video 4. GFP-CD63-transduced WT mouse T lymphoblasts were stimulated with anti-TCR antibody (10 μg/ml; 6 h) bound to IBIDI chamber slides to induce MVB traffic. Video time-lapse experiments (5 frames/sec) showed movement of several GFP-CD63$^+$ vesicles and enhanced cell surface staining (compare Supplementary Video 3) due to TCR-induced vesicle fusion the plasma membrane.

Supplementary Video 5. Magnification of the cell shown in Supplementary Video 4 (right) and tracking of several vesicles (nº 1-4) using ImageJ MJTrack. There is an apparent transient increase in the fluorescence signal at the plasma membrane after vesicle fusion to the membrane (trajectories nº 1 and 2; quantitated in Supplementary Fig. S4).

Supplementary Video 6. GFP-CD63-transduced PKD2$^{-/-}$ T lymphoblasts were plated on fibronection-coated IBIDI chamber slides to image MVB traffic (GFP-CD63$^+$) in unstimulated cells. Video time-lapse experiments as above.

Supplementary Video 7. Synapse formed by a DsRed2-PKD1-expressing Jurkat T lymphocyte (red) with a SEE-loaded (1 μg/ml) , CMAC-labeled Raji B lymphocyte (blue). Both fluorescence channels were captured simultaneously in the video. The red channel was deconvoluted using Huygens Essential Software. DsRed2-PKD1 accumulation was observed at the synaptic contact after 30 min.

Supplementary Video 8. WT mouse T lymphoblasts were challenged with SEB-pulsed (1 μg/ml), CMAC-labeled EL-4 cells (blue) at a 1:1 ratio and transmittance and blue channels were acquired. EL-4 cells were large and blue; T lymphoblasts were smaller and irregular. White arrows indicate synaptic contacts, red arrows indicate cells that show apoptotic blebbing. T, apoptosis of effector T lymphoblasts (AICD); EL4, death of EL-4 target cells (CTL).

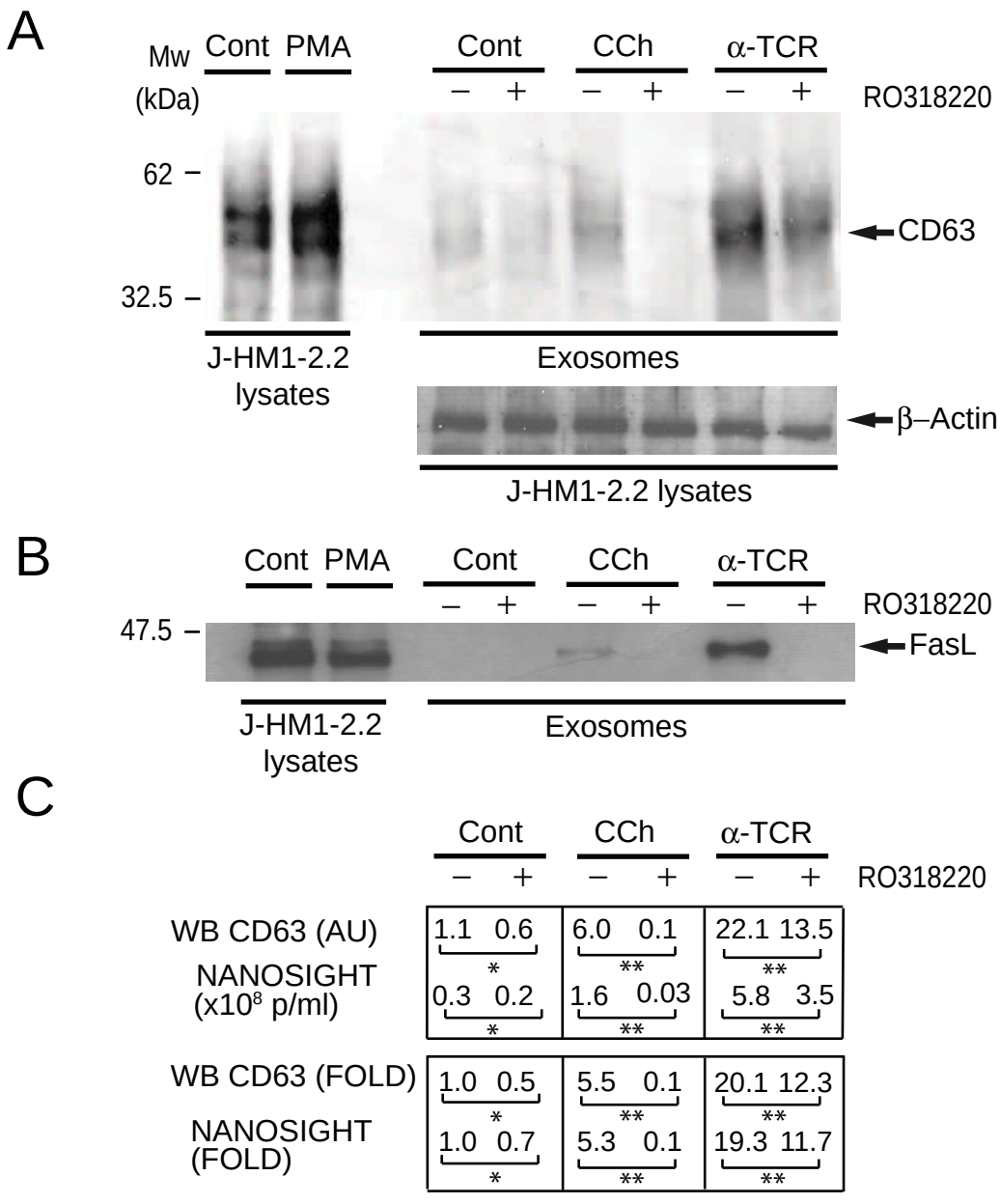

Fig. 1 Mazzeo et al.

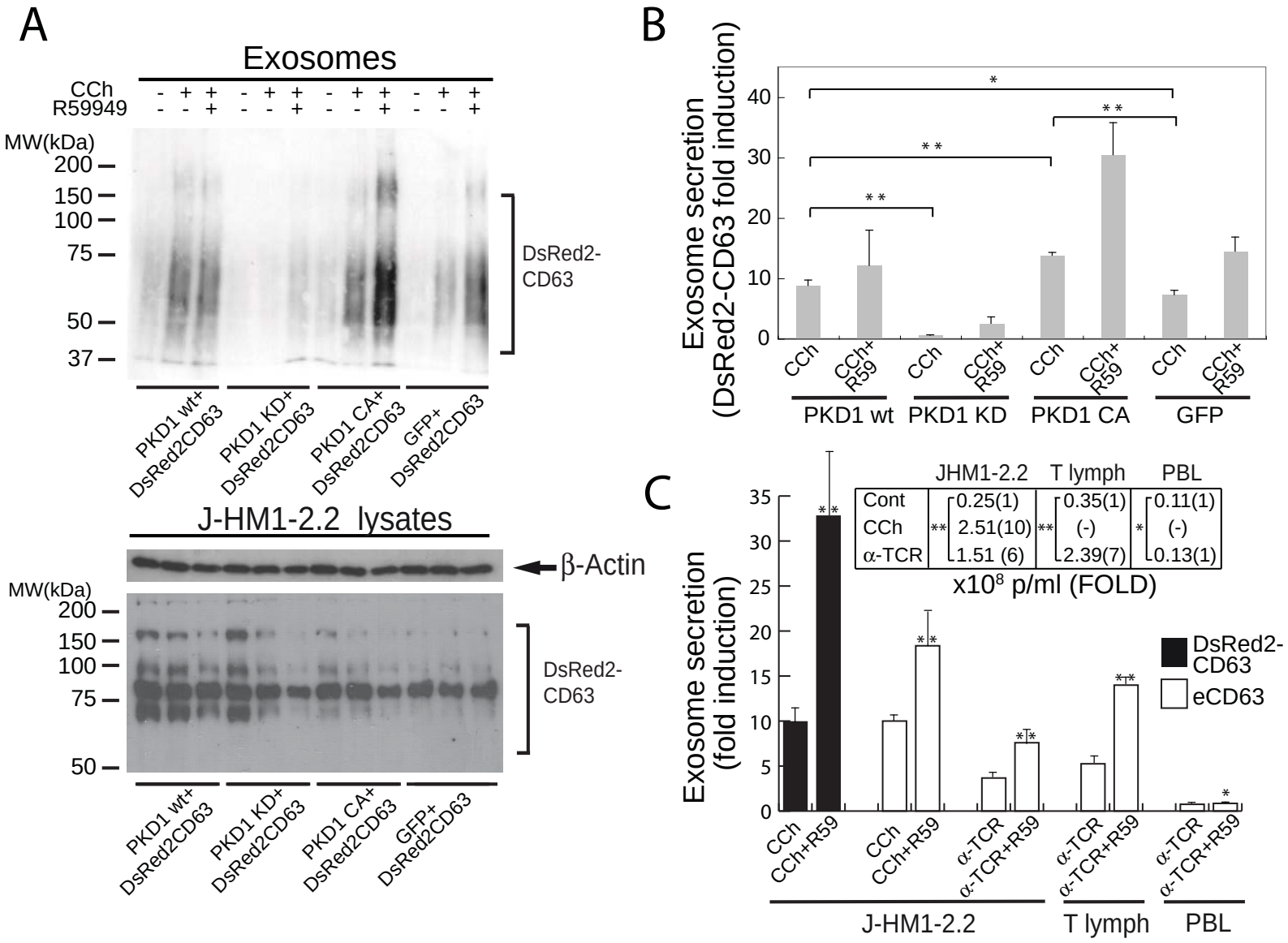

Fig. 2 Mazzeo et al.

A

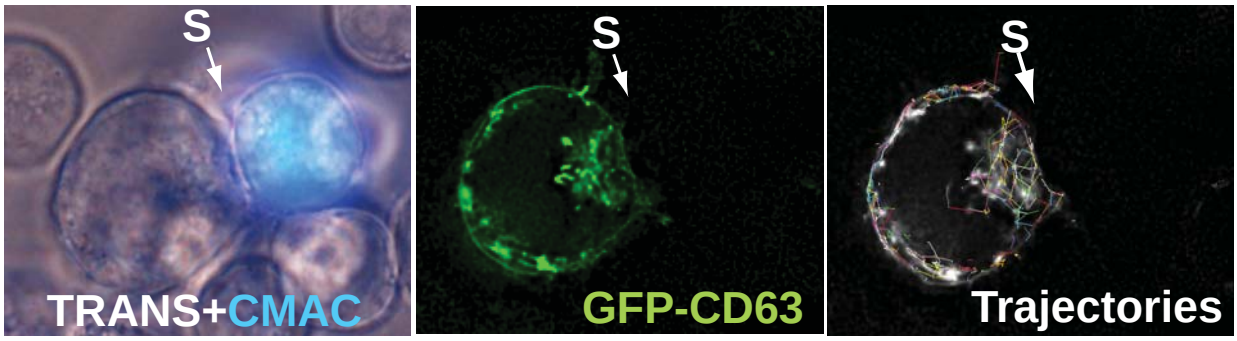

B

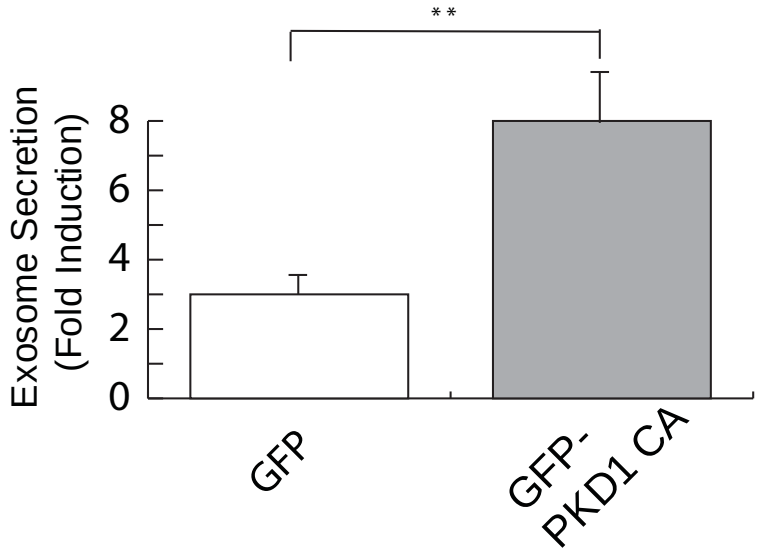

Fig. 3 Mazzeo et al.

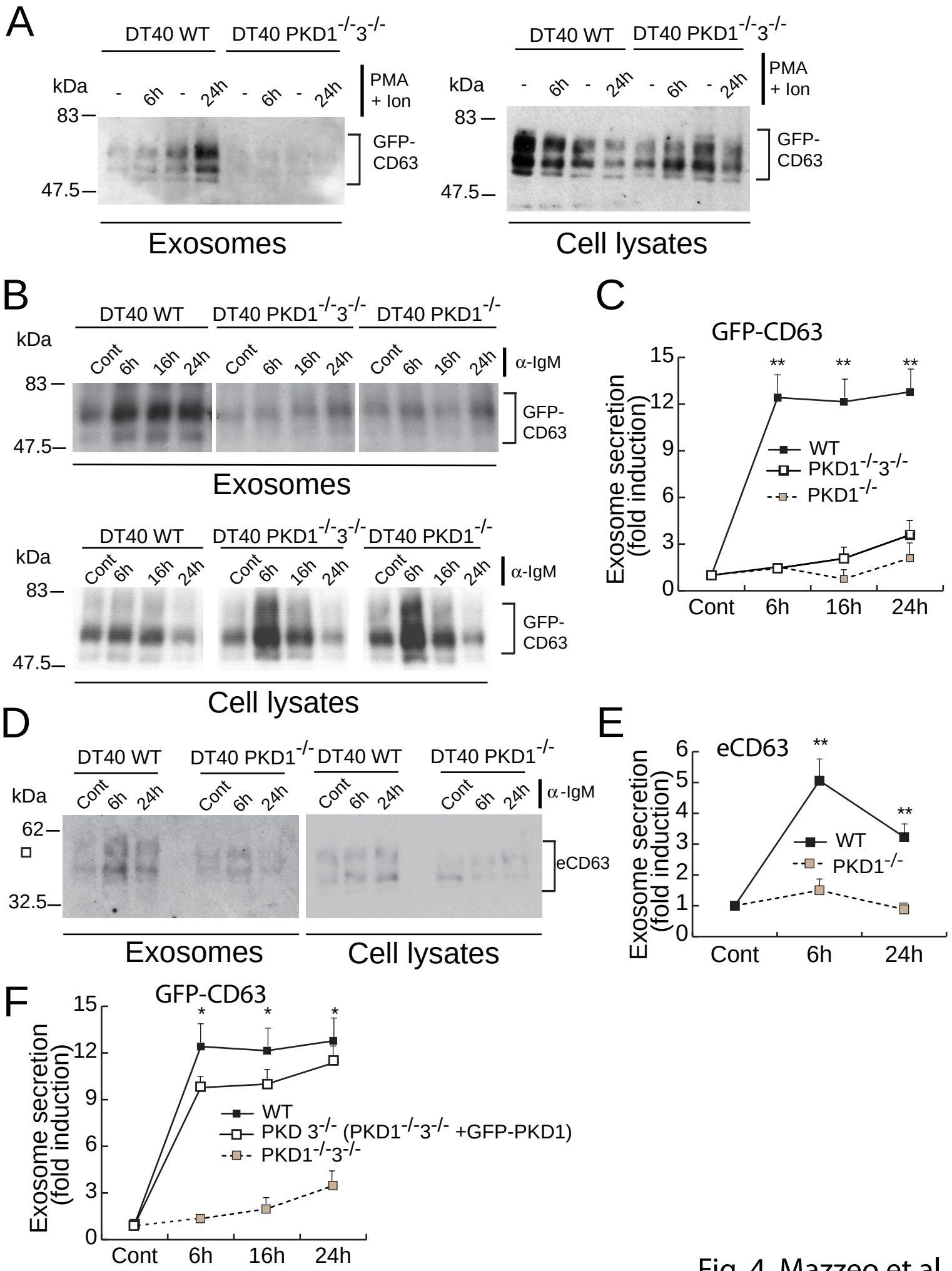

Fig. 4 Mazzeo et al.

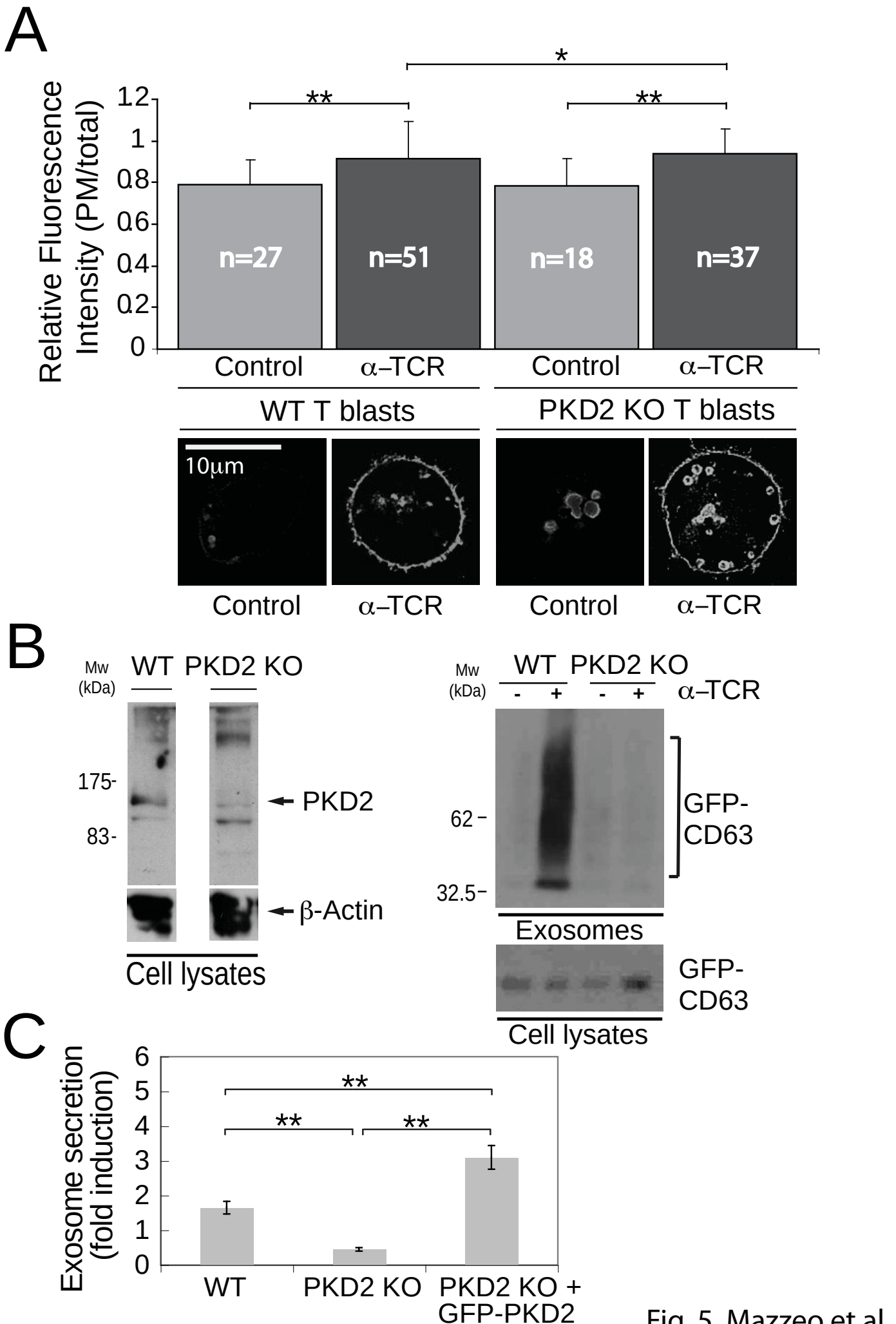

Fig. 5 Mazzeo et al.

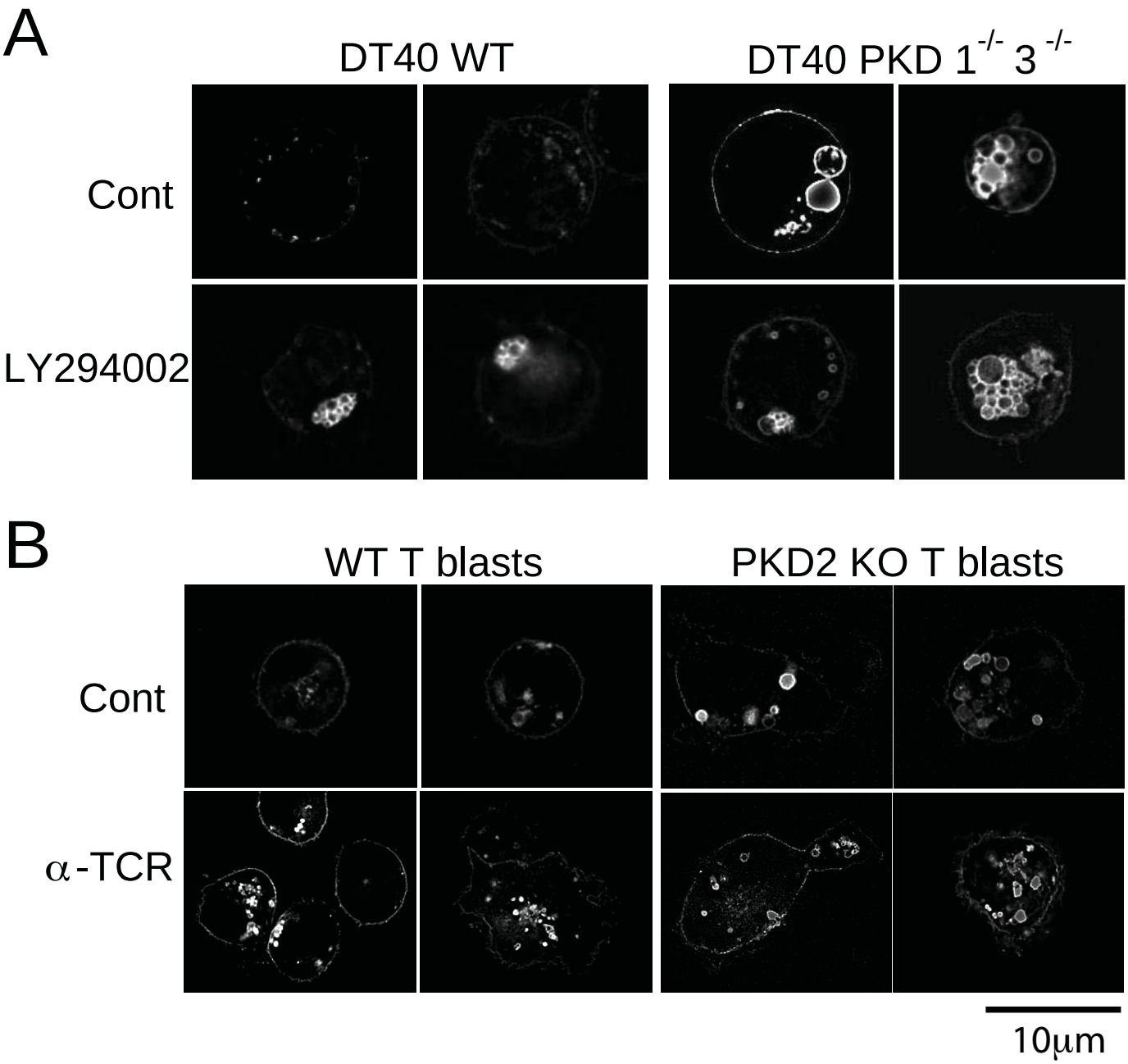

Fig. 6 Mazzeo et al.

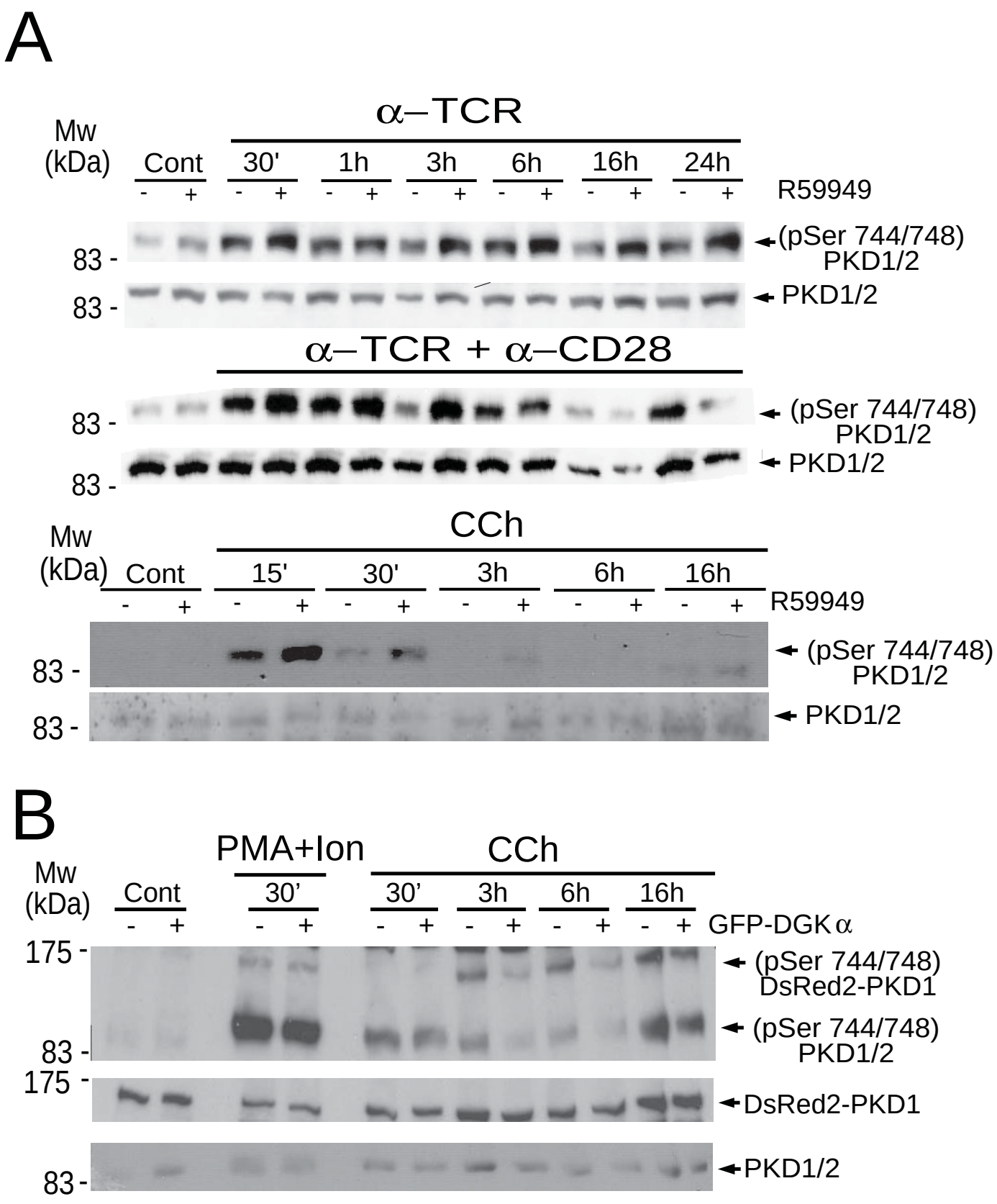

Fig. 7 Mazzeo et al.

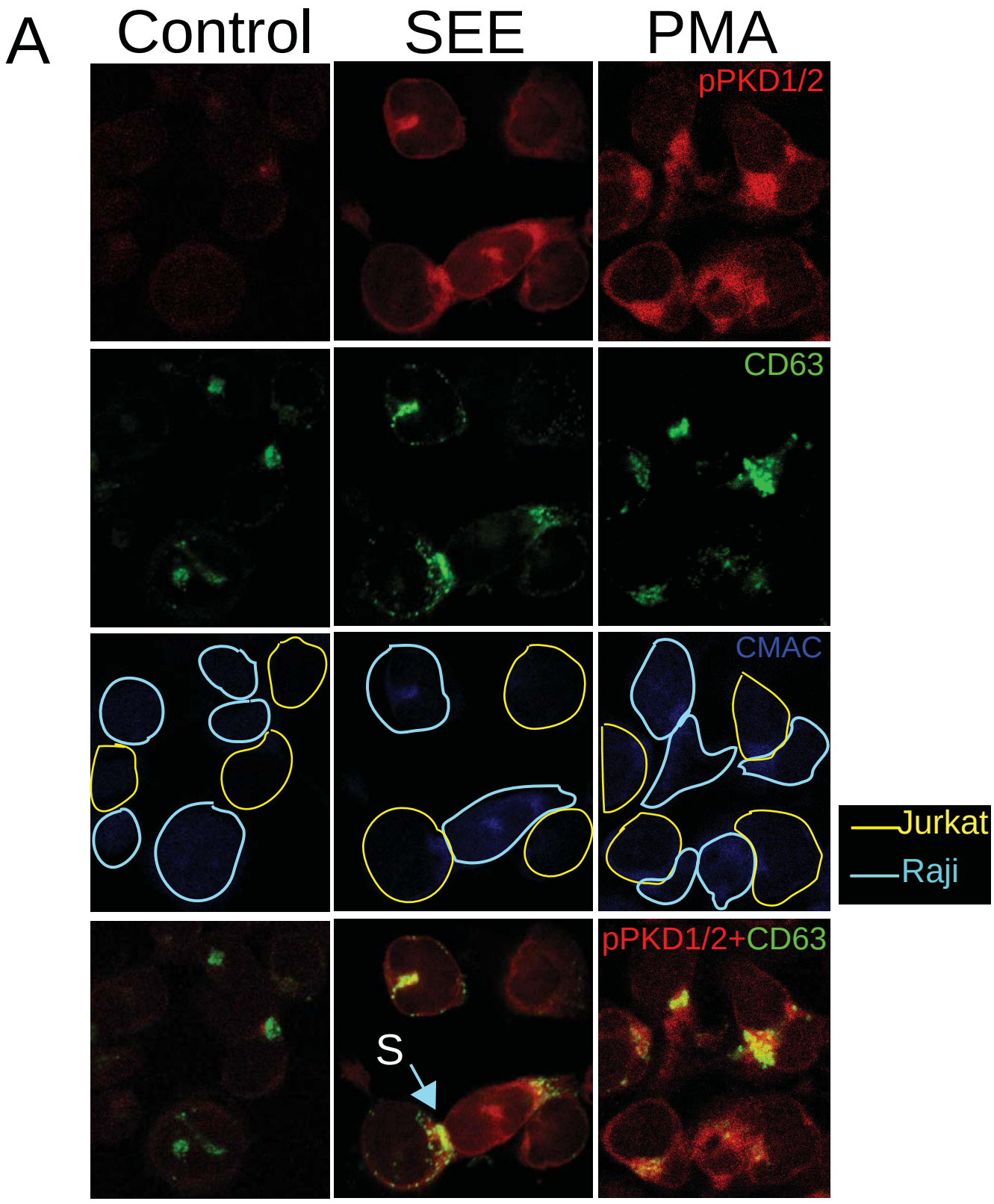

Fig. 8A Mazzeo et al.

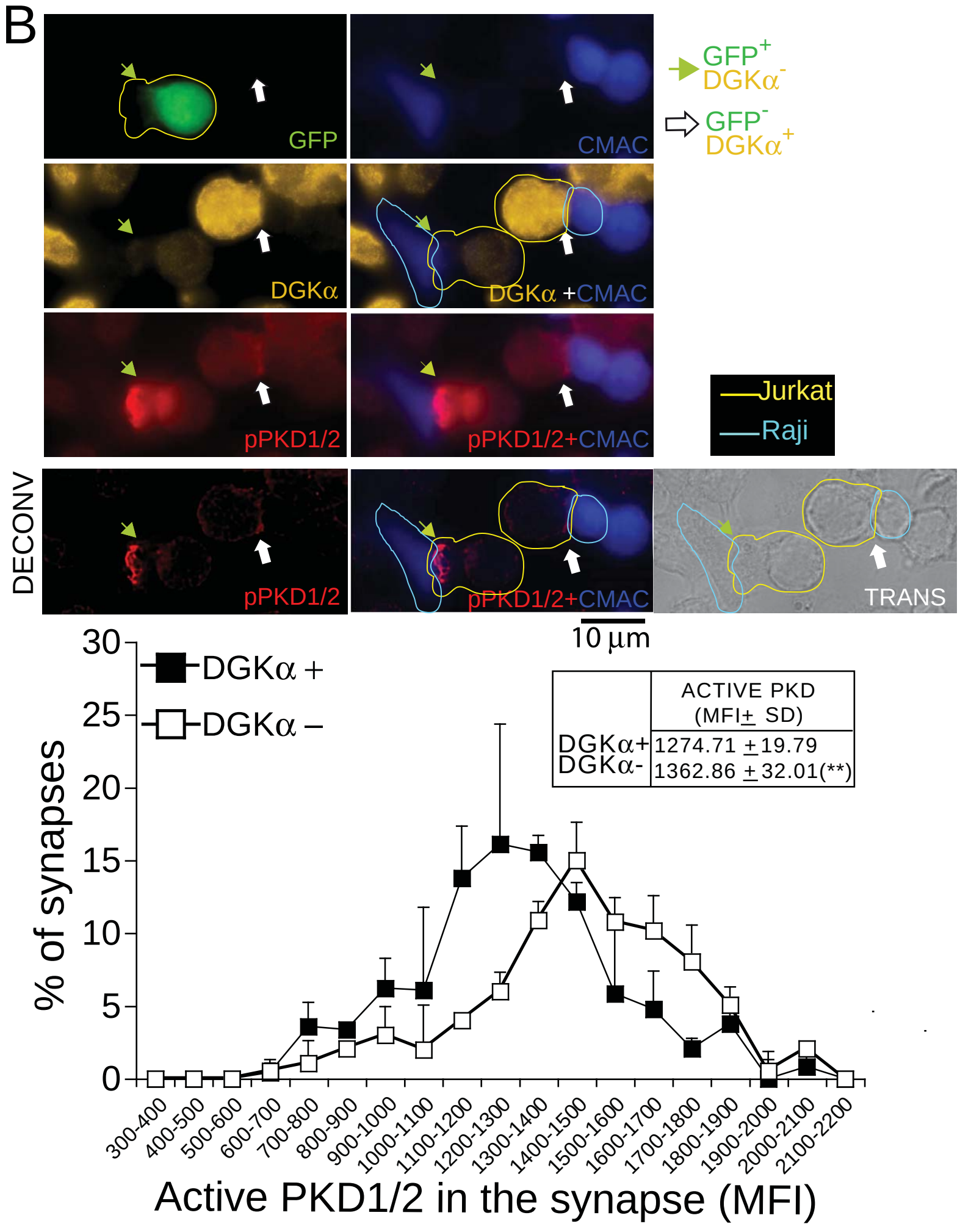

Fig. 8B Mazzeo et al

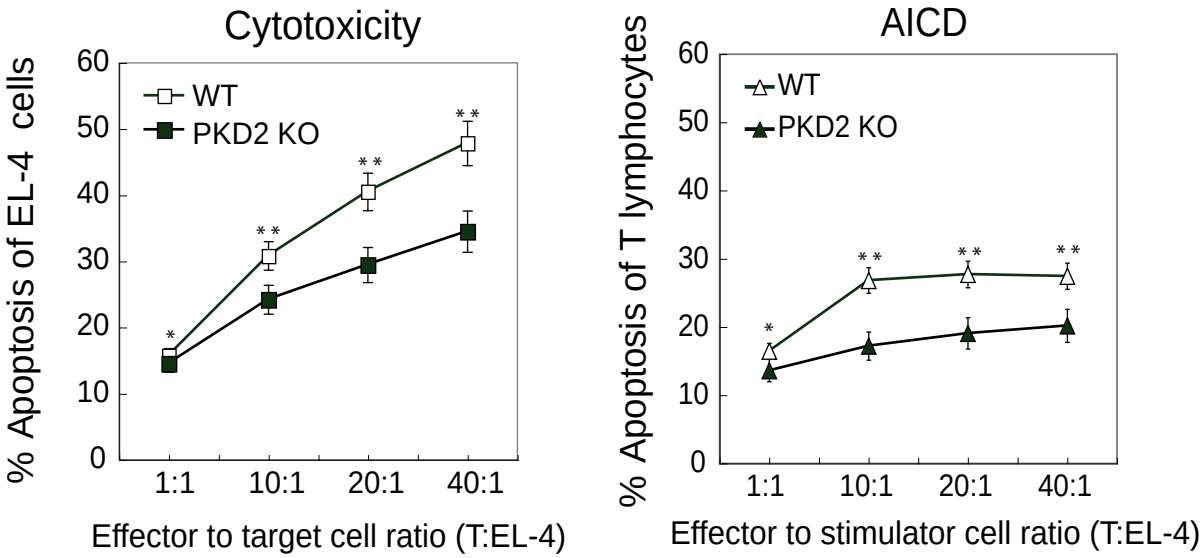

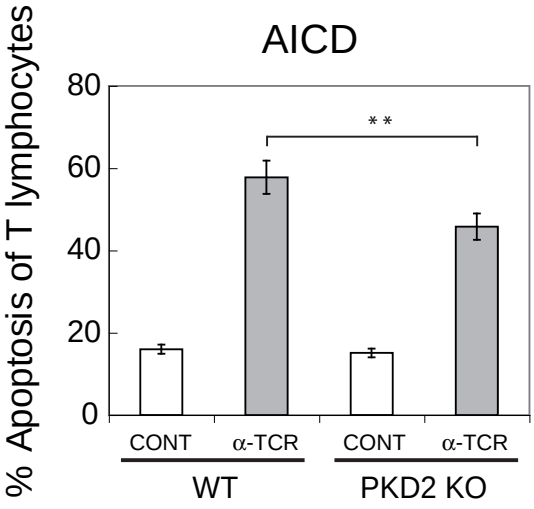

Fig. 9 Mazzeo et al

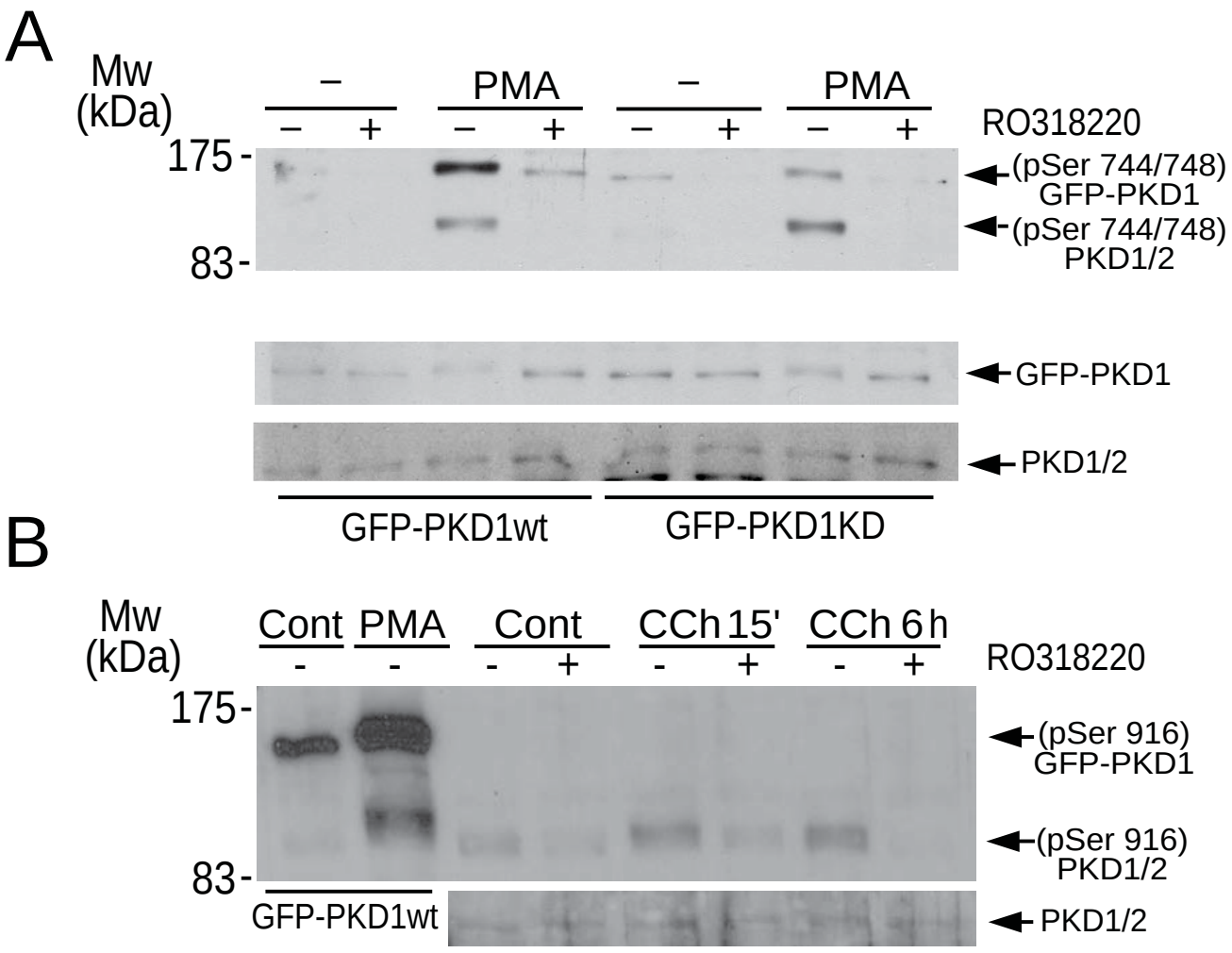

Supplemental Fig S1 Mazzeo et al.

A

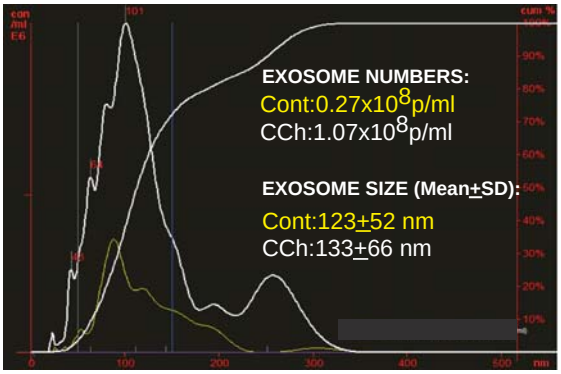

B

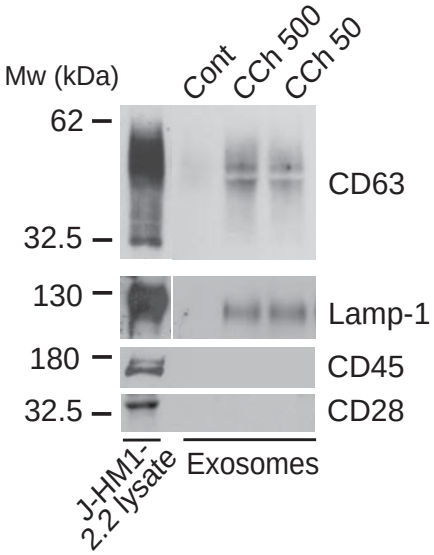

C

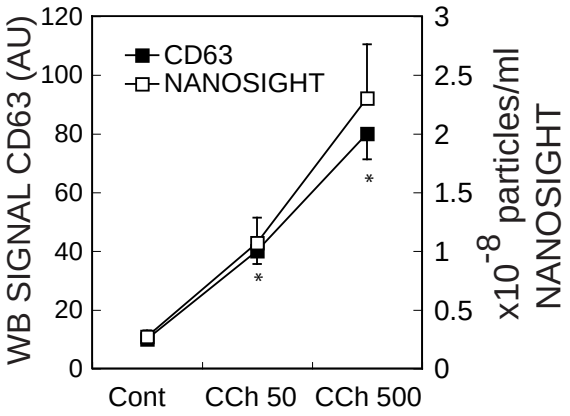

D

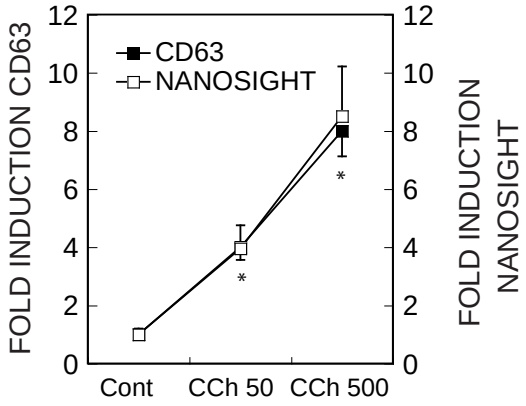

Supplemental Fig. S2 Mazzeo et al.

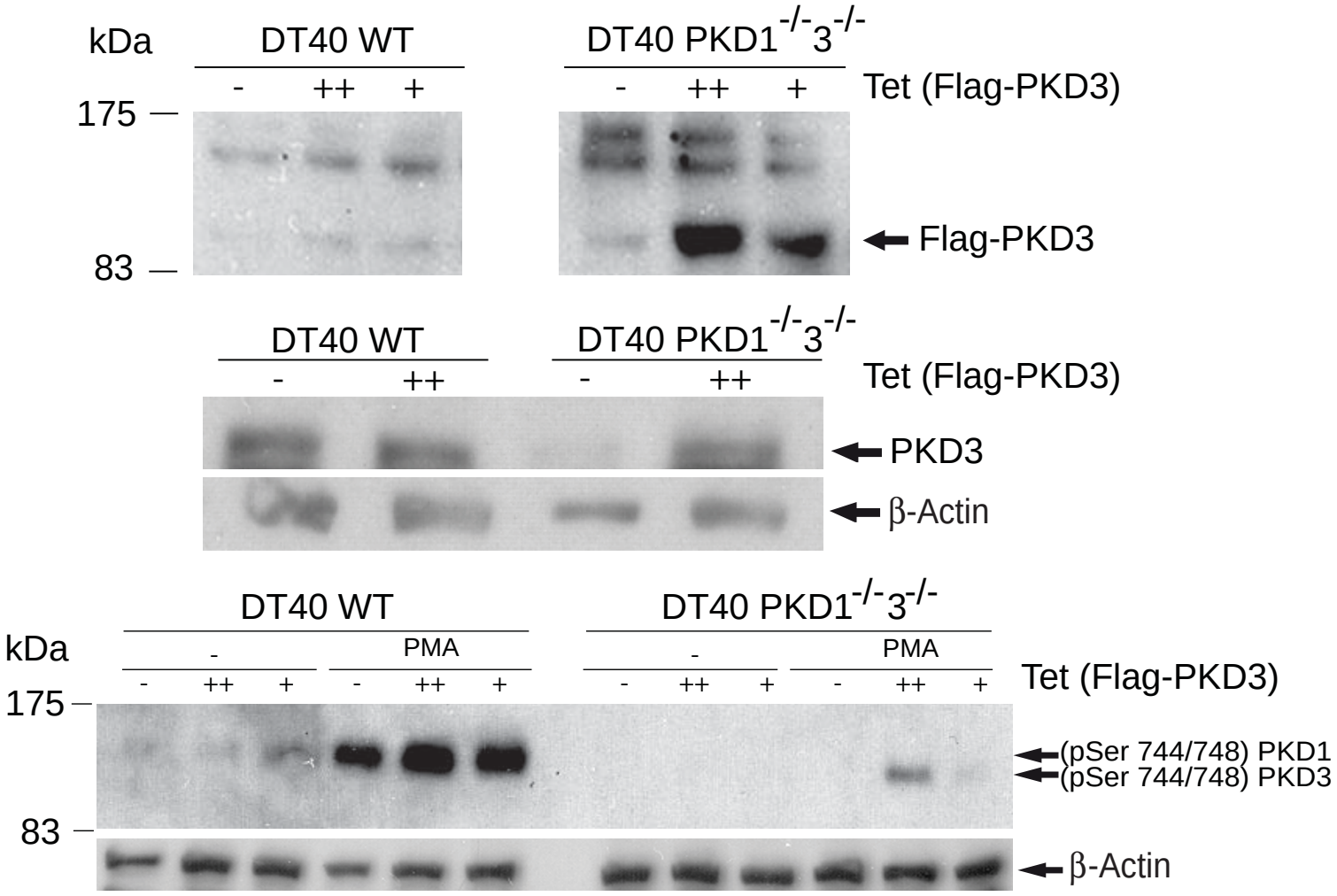

Supplemental figure S3 Mazzeo et al.

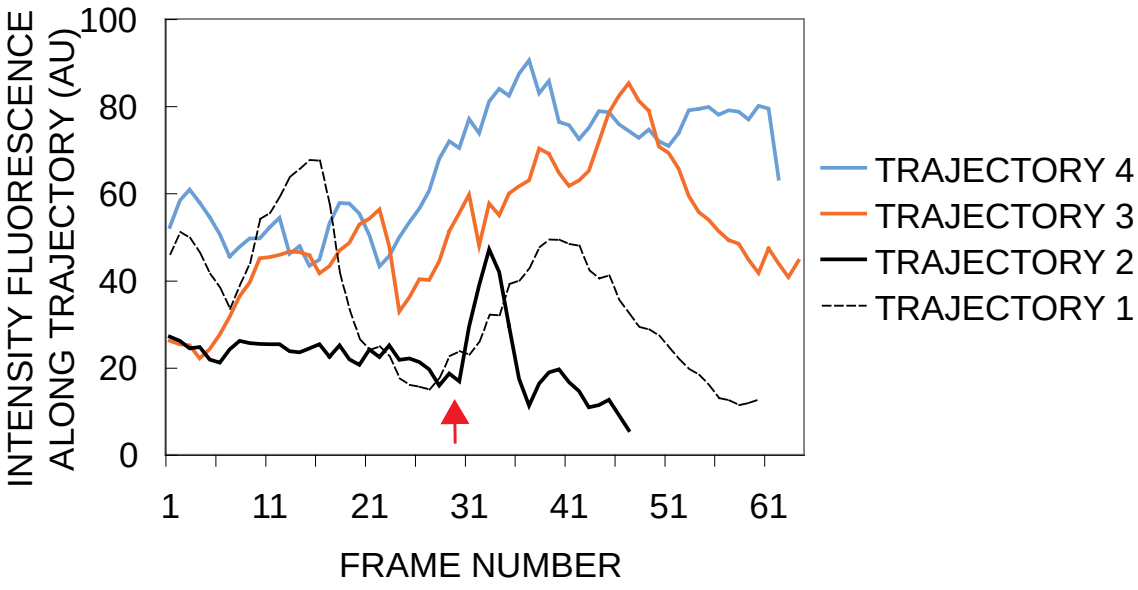

Supplemental figure S4 Mazzeo et al.

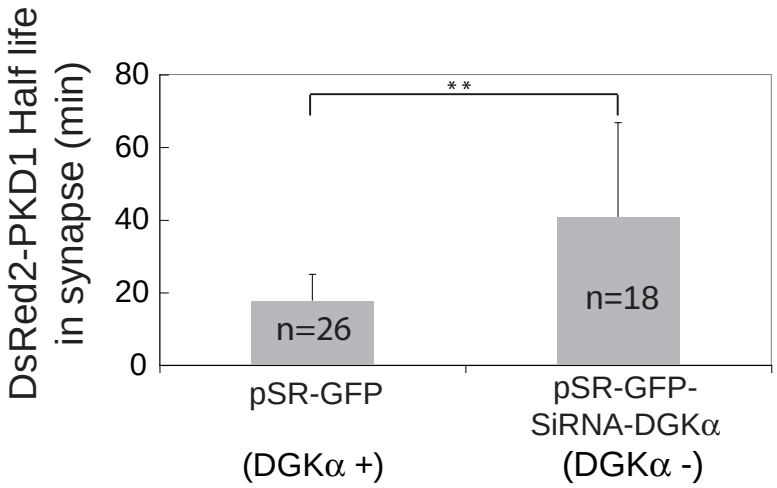

Supplemental Figure S5 Mazzeo at al